Article

CDC7-independent G1/S transition revealed by targeted protein degradation

Jan M. Suski[1,2], Nalin Ratnayeke[3,4], Marcin Braun[1,2,5], Tian Zhang[6], Vladislav Strmiska[1,2], Wojciech Michowski[1,2], Geylani Can[7], Antoine Simoneau[8,9], Konrad Snioch[1,2], Mikolaj Cup[1,2], Caitlin M. Sullivan[1,2], Xiaoji Wu[1,2], Joanna Nowacka[1,2], Timothy B. Branigan[10], Lindsey R. Pack[3,4], James A. DeCaprio[10], Yan Geng[1,2], Lee Zou[8,9], Steven P. Gygi[6], Johannes C. Walter[7], Tobias Meyer[3]✉ & Piotr Sicinski[1,2]✉

The entry of mammalian cells into the DNA synthesis phase (S phase) represents a key event in cell division[1]. According to current models of the cell cycle, the kinase CDC7 constitutes an essential and rate-limiting trigger of DNA replication, acting together with the cyclin-dependent kinase CDK2. Here we show that CDC7 is dispensable for cell division of many different cell types, as determined using chemical genetic systems that enable acute shutdown of CDC7 in cultured cells and in live mice. We demonstrate that another cell cycle kinase, CDK1, is also active during G1/S transition both in cycling cells and in cells exiting quiescence. We show that CDC7 and CDK1 perform functionally redundant roles during G1/S transition, and at least one of these kinases must be present to allow S-phase entry. These observations revise our understanding of cell cycle progression by demonstrating that CDK1 physiologically regulates two distinct transitions during cell division cycle, whereas CDC7 has a redundant function in DNA replication.

The progression of cells through G1 phase and their entry into DNA synthesis (S phase) is one of the most tightly regulated steps of cell division. Mechanisms governing G1/S transition are frequently deregulated in human cancers, and they represent targets of cell-cycle-focused anticancer therapies[1]. During the G1 phase, several proteins assemble on DNA replication origins and form pre-replication complexes that wait for a signal to trigger origin firing. This signal is thought to be provided by the kinase CDC7, which acts in concert with cyclin E−CDK2 (refs. [2,3]). The major function of CDC7 is to phosphorylate MCM proteins within pre-replication complexes[4–8]. This, together with the action of cyclin E−CDK2, promotes binding of CDC45 and GINS to MCM2–7, which results in the formation of the CDC45−MCM−GINS (CMG) complex and activation of DNA helicase. These events cause unwinding of double-stranded DNA, recruitment of DNA polymerase and initiation of DNA synthesis[9].

CDC7 is a highly conserved serine-threonine kinase activated through interaction with its regulatory subunit DBF4 (refs. [4–8]). According to current models of the cell cycle, CDC7 represents an essential component of the cell cycle machinery that is indispensable for S-phase entry in all organisms studied[10].

We decided to revisit this notion using two independent chemical genetic approaches: the analogue-sensitive inhibition approach and the generation of cells and mice that allow highly specific and acute targeted degradation of CDC7 protein in vitro and in vivo.

Cell proliferation without CDC7

To re-assess the requirement for CDC7 in cell proliferation, we first generated an analogue-sensitive (as) version of CDC7 by mutating the bulky gatekeeper residue in the ATP-binding pocket of CDC7 from Met128 to glycine. This substitution creates an enlarged ATP-binding pocket not found in wild-type kinases. While the analogue-sensitive substitution does not alter kinase specificity[11], the substituted kinase can be selectively inhibited by bulky chemical compounds such as 1NM-PP1 or 3MB-PP1 that occupy the enlarged ATP-binding pocket[12] (Extended Data Fig. 1a). Importantly, as inhibitors do not inhibit wild-type kinases. We knocked-in the asCDC7 mutation into the endogenous Cdc7 locus in mouse embryonic stem (ES) cells and generated homozygous CDC7[AS/AS] cells (Extended Data Fig. 1b). Unexpectedly, acute inhibition of CDC7 in CDC7[AS/AS] cells with 1NM-PP1 did not arrest proliferation, although cell growth was retarded (Fig. 1a). By contrast, similar inhibition of CDK1, an essential kinase for cell proliferation[13], using CDK1[AS/AS] ES cells[12], completely arrested cell growth (Extended Data Fig. 1c, d).

To test the requirement for the CDC7 kinase in another cell type, we injected CDC7[AS/AS] ES cells into mouse blastocysts and generated CDC7[AS/AS] embryos, from which we derived mouse embryonic fibroblasts (MEFs). Again, CDC7[AS/AS] MEFs continued to proliferate despite acute CDC7 inhibition with 1NM-PP1 (Fig. 1b).

[1]Department of Cancer Biology, Dana–Farber Cancer Institute, Boston, MA, USA. [2]Department of Genetics, Blavatnik Institute, Harvard Medical School, Boston, MA, USA. [3]Department of Cell and Developmental Biology, Weill Cornell Medicine, New York, NY, USA. [4]Department of Chemical and Systems Biology, Stanford University, Stanford, CA, USA. [5]Department of Pathology, Chair of Oncology, Medical University of Lodz, Lodz, Poland. [6]Department of Cell Biology, Harvard Medical School, Boston, MA, USA. [7]Department of Biological Chemistry and Molecular Pharmacology, Harvard Medical School, Boston, MA, USA. [8]Massachusetts General Hospital Cancer Center, Harvard Medical School, Charlestown, MA, USA. [9]Department of Pathology, Massachusetts General Hospital, Harvard Medical School, Boston, MA, USA. [10]Department of Medical Oncology, Dana–Farber Cancer Institute, Boston, MA, USA. ✉e-mail: tom4003@med.cornell.edu; peter_sicinski@dfci.harvard.edu
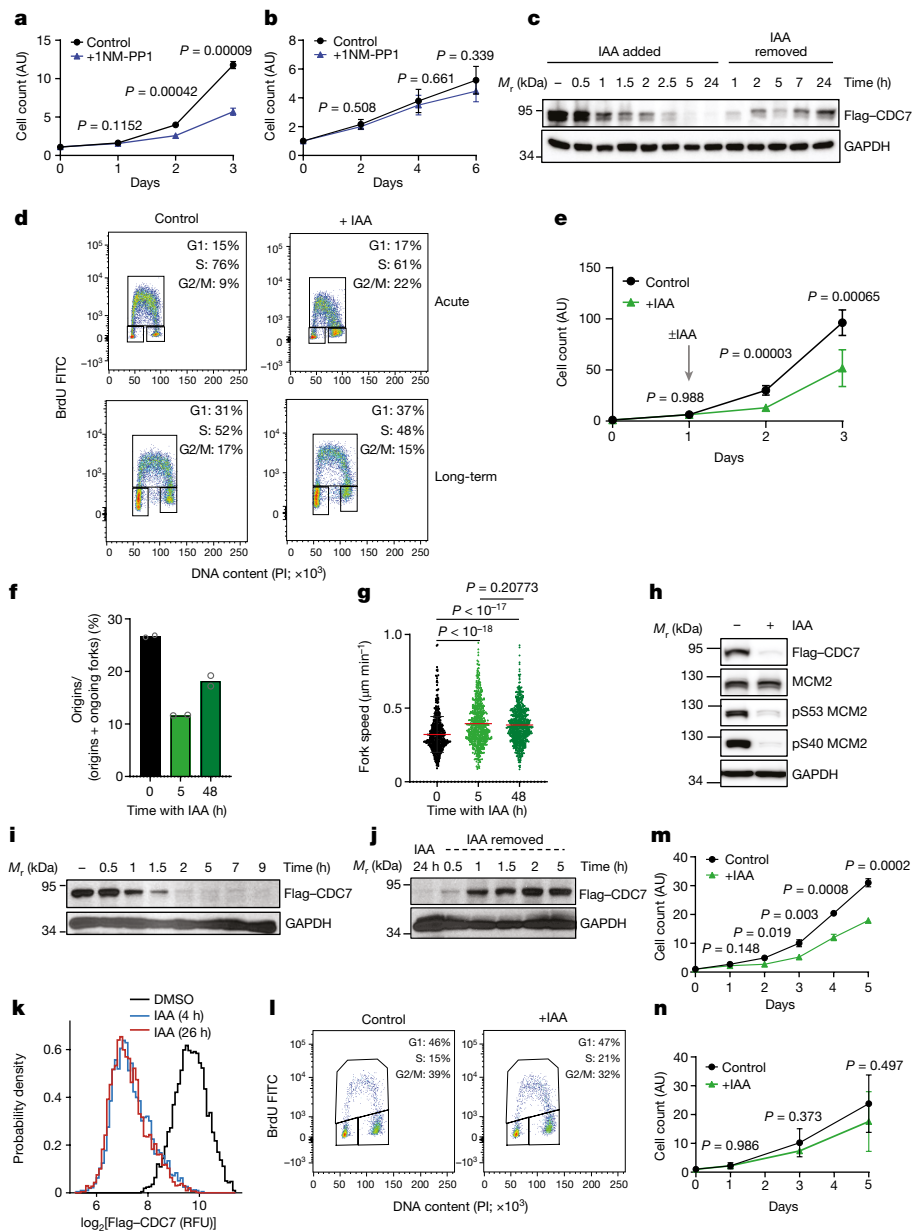
Fig. 1 | Shut down of CDC7 in cultured cells. a, **b**, Growth curves of CDC7^AS/AS ES cells (**a**) and MEFs (**b**) cultured with 1NM-PP1 (to inhibit CDC7) or with vehicle (control). AU, arbitrary units. **c**, Western blot analysis of CDC7 protein levels in CDC7^AID/AID ES cells treated with auxin (IAA). **d**, Flow cytometry of CDC7^AID/AID/TIR1 ES cells treated with IAA for 12 h (acute) or 48 h (long-term). PI, propidium iodide. **e**, Growth curves of CDC7^AID/AID/TIR1 ES cells. Starting at day 1, cells were treated with IAA or vehicle. **f**, **g**, DNA fibre analysis, with the mean fraction of new replication origins (**f**) and fork speed (**g**) in CDC7^AID/AID/TIR1 ES cells treated with IAA for the indicated times. **h**, Western blot analysis of phospho-MCM2 residues in CDC7^AID/AID/TIR1 ES cells treated with IAA for 2 days. **i**, **j**, Western blot analysis of CDC7 protein levels in CDC7^AID/AID/TIR1 MEFs treated with IAA (**i**) or after IAA removal (**j**). **k**, Immunofluorescence analysis of CDC7^AID/AID/TIR1 MEFs treated for 4 or 26 h with IAA or vehicle (dimethyl sulfoxide (DMSO)) and stained for Flag–CDC7. **l**, Flow cytometry of CDC7^AID/AID/TIR1 MEFs treated with IAA or vehicle for 2 days. **m**, Growth curves of CDC7^AID/AID/TIR1 MEFs cultured in the presence of IAA or vehicle **n**, Growth curves of CDC7^AID/AID/TIR1 MEFs immortalized by dominant-negative p53, cultured with IAA or with vehicle. For **a**, **b**, **e**, **f**, **g**, **m** and **n**, mean values are shown, with error bars representing the s.d. P values were determined by two-sided t-test. For **a**, **b**, **e**, **m** and **n**, $n = 3$ independent replicates; **f**, $n = 2$; **g**, $n > 500$ cells; **c**, **d**, **h**–**k**, representative results (out of 2) are shown.

To extend these findings, we generated a system to acutely remove CDC7 protein. We adopted the auxin-inducible degradation (AID) approach[14]. This plant-derived system can be transplanted into mammalian cells by inserting the AID domain into the protein of interest, together with simultaneous expression of the plant F-box protein Tir1 (ref. [14]) (Extended Data Fig. 1e). Administration of auxin (indole acetic acid (IAA)) to cells engineered in this fashion triggers an acute degradation of the AID-tagged protein. This system has been used to degrade proteins in cultured cells, but not to target endogenous proteins in a living animal. We knocked-in the AID domain into the endogenous *Cdc7* locus in ES cells and generated CDC7^AID/AID cells (Extended Data Fig. 1f, g). In addition, we knocked-in the *Tir1* gene into the ubiquitously expressed *Rosa26* locus (Extended Data Figs. 1h–k and 2a, b).

Treatment of in vitro cultured CDC7^AID/AID/TIR1 ES cells with IAA led to a rapid loss of CDC7 protein (Fig. 1c). Degradation of CDC7 was accompanied by strong decrease in levels of the CDC7 regulatory subunit, DBF4, which suggests that DBF4 is unstable in the absence of its catalytic partner (Supplementary Table 1). Acute shutdown of

CDC7 resulted in a modest delay in cell cycle progression, which lasted approximately 24 h, after which cells resumed essentially normal proliferation (Fig. 1d, e and Extended Data Fig. 2c; also see below). DNA fibre analysis revealed a decrease in the number of new replication origins (Fig. 1f), which was compensated by an increased speed of existing forks (Fig. 1g). By 48 h, however, the number of new origins partially recovered, despite continued depletion of CDC7 (Fig. 1f, g and Extended Data Fig. 2d). Analysis of MCM2 phosphorylation revealed strongly reduced phosphorylation of CDC7-dependent residues, which persisted as long as IAA was present (Fig. 1h). We cultured cells in the presence of IAA for up to 7 weeks and observed that they proliferated normally and maintained efficient depletion of CDC7 (Extended Data Fig. 2d).

To extend these observations to another cell type, we injected CDC7[AID/AID]/TIR1 ES cells into blastocysts and derived CDC7[AID/AID]/TIR1 MEFs. Treatment of MEFs with IAA resulted in efficient degradation of CDC7 within 2 h (Fig. 1i, k and Extended Data Fig. 2e), and this effect was reversible following removal of IAA (Fig. 1j). Acute shutdown of CDC7 resulted in transient and mild impairment of cell proliferation, followed by the return of normal proliferation rates (Fig. 1l, m).

Inactivation of p53 is thought to render cells particularly vulnerable to CDC7 inhibition[15,16]. To test this, we immortalized CDC7[AID/AID]/TIR1 MEFs using dominant-negative p53 and then degraded CDC7. Again, these cells continued to proliferate despite CDC7 shutdown (Fig. 1n).

To better delineate the impact of CDC7 inhibition on the first and successive cell cycles, we performed live-cell imaging of CDC7[AID/AID]/TIR1 MEFs acutely treated with IAA and human mammary epithelial MCF10A cells treated with a CDC7 inhibitor. We observed lengthening of S phase and modest prolongation of G1 and G2 phases during the first cell cycle, which resulted in an increased duration of the first cell division. These parameters returned to nearly normal length in the second or third cell cycles (Fig. 2a–c and Extended Data Fig. 3a–f). Consistent with live-cell imaging, pulse-chase analyses of ES cells and MEFs treated with IAA, as well as human cells treated with a CDC7 inhibitor, revealed lengthening of cell cycle phases at 12–24 h after CDC7 degradation or inhibition, which resulted in increased cell division time. These parameters returned to nearly normal length after 48–72 h of continuous CDC7 inhibition (Fig. 2d–g and Extended Data Fig. 3g–j). We did not observe increased cell death after CDC7 degradation or inhibition (Fig. 2h, i and Extended Data Fig. 3k–n). The numbers of γH2AX foci were slightly increased in ES cells, but not in MEFs, shortly after CDC7 depletion (Extended Data Fig. 3o, p, r), and ES cells cultured in the presence of IAA for 7 weeks did not display increased numbers of γH2AX foci (Extended Data Fig. 3q). We concluded that acute CDC7 inhibition results in transient lengthening of the cell cycle but no substantial DNA damage or cell death.

It was possible that the vanishingly small amounts of CDC7 activity left after IAA treatment (or after inhibition of analogue-sensitive CDC7) were sufficient to allow cell proliferation. To test this, we used CRISPR–Cas9 to knockout CDC7 in different mouse and human cell types. We also generated Cdc7[Flox/Flox] murine ES cells by gene targeting (Extended Data Fig. 1l), and acutely shutdown CDC7 in these cells by expression of Cre-recombinase. In all the cell types tested, we observed continued cell cycle progression despite knocking out CDC7 (Extended Data Fig. 4). We also observed that proliferating primary mouse cardiomyocytes do not express detectable CDC7 protein (Extended Data Fig. 5a, b). Last, we used CRISPR–Cas9 to knockout the activator of CDC7, Dbf4, in immortalized mouse fibroblasts. Dbf4-null cells continued to proliferate, albeit at a modestly reduced rate (Extended Data Fig. 5c–g). Collectively, these observations reveal that CDC7 is dispensable for proliferation in several cell types.

To extend these studies in vivo, we generated CDC7[AID/AID]/TIR1 mice using standard methods. Probing of a panel of mouse organs with an anti-Flag antibody (which detects endogenous Flag-tagged CDC7[AID]) revealed that CDC7 is expressed at very low levels in most organs, including no detectable CDC7 protein in proliferative bone marrow (Extended Data Fig. 5h–j). Administration of IAA to adult CDC7[AID/AID]/TIR1 mice led to efficient depletion of CDC7 in their internal organs starting at 3–6 h (Extended Data Fig. 5k–l), and this effect persisted throughout the entire length of the study (Extended Data Fig. 5m). Prolonged shutdown of CDC7 did not result in any visible phenotypes and did not impede proliferation of mitotically active compartments (Extended Data Fig. 5n, o). We concluded that CDC7 is largely dispensable in cultured cells and in live mice.

Synergy between CDC7 and CDK1

We wanted to understand the molecular basis of cell proliferation in the absence of CDC7. Since CDK2 has been postulated to play a role with CDC7 in the firing of DNA replication origins[2,3], we considered the possibility that in the absence of CDC7, CDK2 alone can drive the entry of cells into S phase. Cdk2-null mice are viable, which indicates that CDK2 is not essential for DNA synthesis[17,18]. We used CRISPR–Cas9 to generate Cdk2 knockout CDC7[AID/AID]/TIR1 ES cells or CDK2 knockout human mammary epithelial HMEC and MCF10A cells. We also engineered human cells to express analogue-sensitive CDK2 in place of the endogenous CDK2. Combined ablation of CDK2 (or acute inhibition of CDK2 kinase) plus degradation or inhibition of CDC7 did not block asynchronous cell proliferation and had little effect on S-phase entry in cells returning from quiescence (Fig. 3a–c and Extended Data Fig. 6). We concluded that another kinase may act at G1/S to drive S-phase entry.

To identify this kinase, we acutely degraded CDC7 in CDC7[AID/AID]/TIR1 cells and used quantitative mass spectrometry to gauge the phosphorylation status of MCM proteins, which are well-established targets of CDC7 (refs. [4–8]). Phosphorylation of known CDC7-specific sites and sites sharing the CDC7 consensus sequence (acidic amino acid directed) within MCM proteins was strongly decreased following CDC7 depletion (Fig. 3d and Supplementary Table 2). By contrast, several other MCM sites remained phosphorylated in CDC7-depleted cells (Supplementary Table 2). Normal phosphorylation of Ser27 of MCM2 in CDC7-depleted cells and in CDC7-depleted/Cdk2-knockout cells was confirmed by immunoblotting with a phosphospecific antibody (Fig. 3e). Several of these CDC7-independent sites represent predicted substrates for proline-directed kinases. Therefore, we hypothesized that another proline-dependent kinase might be responsible for their phosphorylation.

Further analyses of the CDC7-depleted phosphoproteome (Supplementary Table 2) revealed changes indicative of increased CDK1 kinase activity (increased phosphorylation of activating Thr161 and decreased phosphorylation of inhibitory Thr15 sites of CDK1 (Extended Data Fig. 7a)). Immunoprecipitation of CDK1 followed by kinase assays confirmed mildly increased CDK1 activity in CDC7-deficient cells (Extended Data Fig. 4p and Extended Data Fig. 7b). These observations led us to hypothesize that CDK1 might be responsible for phosphorylating MCM proteins in vivo, as suggested by previous studies[19–21]. Consistent with this, we found that CDK1, but not CDC7, can phosphorylate Ser27 of MCM2 (Extended Data Fig. 7c).

To test whether CDK1 phosphorylates MCM proteins in cells under physiological conditions, we utilized CDK1[AS/AS] knock-in ES cells that express analogue-sensitive CDK1 (ref. [12]). Analogue-sensitive kinases can use N^6-substituted bulky ATP analogues, whereas wild-type kinases cannot use them owing to steric hindrance. Hence, by providing cells that express analogue-sensitive kinase with bulky ATP analogues in which gamma-phosphate has been replaced with thiophosphate, one can label direct substrates of this kinase with a thiophosphate tag[12]. We cultured CDK1[AS/AS] cells in the presence of a bulky ATPγS analogue, which resulted in the labelling of CDK1 substrates. We then immunoprecipitated endogenous MCM2 and probed immunoblots with an anti-thiophosphate ester antibody. These analyses confirmed that CDK1 directly phosphorylates MCM2 in cells (Fig. 3f). Moreover, inhibition of CDK1 kinase in CDK1[AS/AS] cells with 3MB-PP1 decreased the phosphorylation of endogenous MCM2 on Ser27 (Extended Data Fig. 7d).
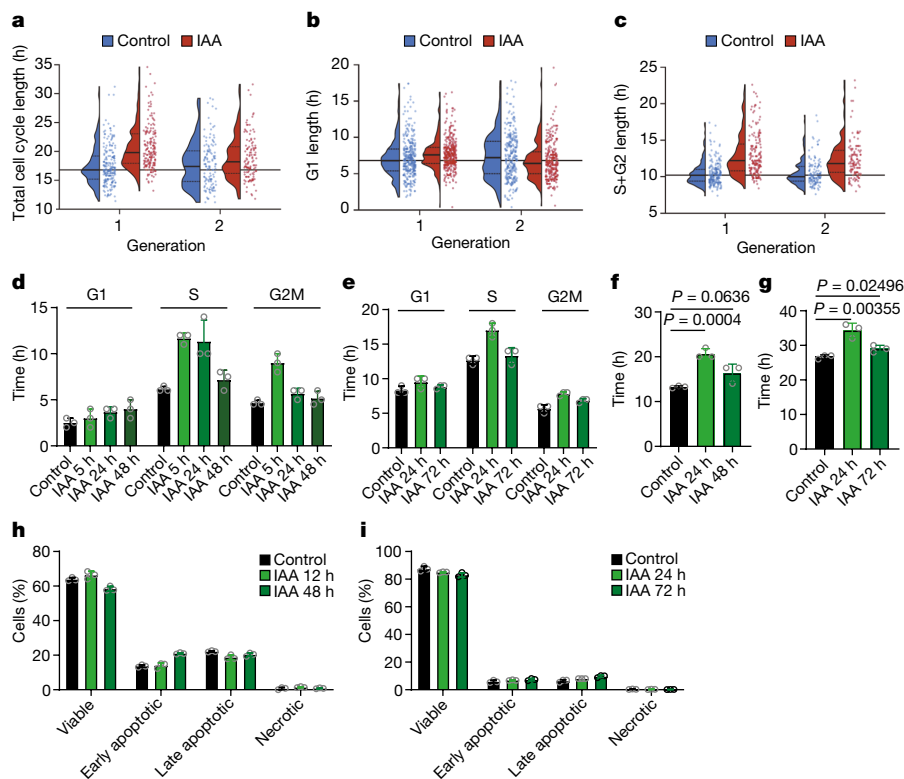
Fig. 2 | Analyses of cells following CDC7 degradation. a–c, Long-term live-cell imaging. Immortalized CDC7$^{AID/AID}$/TIR1 MEFs expressing Gem$^{(1–110)}$–mCherry and Cdt1$^{(1–100)Cy(–)}$–mVenus FUCCI(CA) cell cycle reporters were cultured and imaged for a total of 77 h. Seven hours after imaging start, cells were treated with auxin (IAA) or vehicle (control) and imaged for an additional 70 h. Shown are parameters for the first two cell cycles (generations 1 and 2) after addition of IAA (selecting cells that received IAA 0–4 h before mitosis). **a,** Total cell cycle length (time between mitoses). **b,** G1 length (time between mitosis and Cdt1$^{(1–100)Cy(–)}$ $_{drop}$; that is, start of S phase). **c,** S/G2 length (time from Cdt1$^{(1–100)Cy(–)}$ $_{drop}$ to subsequent mitosis). Dots show values for individual cells; horizonal lines, median values; dotted lines, the inter-quartile range; and the long horizonal line, the median value from control cells in generation 1.

d, e, Length of cell cycle phases determined by pulse-chase in CDC7$^{AID/AID}$/TIR1 ES cells (**d**) and MEFs (**e**) treated for the indicated times with IAA. The control represents the length of cell cycle phases in untreated cells. **f, g,** Doubling times of CDC7$^{AID/AID}$/TIR1 ES cells (**f**) and MEFs (**g**) treated for the indicated times with IAA, determined by pulse-chase. The control represents the doubling time of untreated cells. **h, i,** Percentages of viable (annexin V$^-$PI$^-$), early apoptotic (annexin V$^+$PI$^-$), late apoptotic (annexin V$^+$PI$^+$) and necrotic (annexin V$^-$PI$^+$) CCD7$^{AID/AID}$/TIR1 ES cells (**h**) and MEFs (**i**) treated with IAA for the indicated times. The control represents untreated cells. For **d–i**, bars denote mean values, with error bars representing the s.d. *P* values were determined by two-sided *t*-test. *n* = 3 independent replicates.

According to current models of the cell cycle, CDK1 kinase operates during mitosis and in late S phase[1]. However, CDK1 has not been implicated in normal G1/S transition. To test whether CDK1 is physiologically active during S-phase entry, we synchronized wild-type mouse ES cells in M phase with nocodazole, released the cells and followed their synchronous exit from mitosis and progression through G1 and S phases (Extended Data Fig. 7e). We then immunoprecipitated CDK1 at different time points and quantified its kinase activity. Notably, we detected induction of CDK1 kinase in cells entering S phase (Fig. 3g). We also synchronized CDK1$^{AS/AS}$ cells as described above, and provided cells entering S phase with a bulky ATPγS analogue to label CDK1 substrates. This approach confirmed that CDK1 is active and it directly phosphorylates MCM2 at this cell cycle stage (Extended Data Fig. 7f).

We also rendered mouse and human cells quiescent by serum deprivation, and then stimulated them to re-enter the cell cycle (Extended Data Fig. 7g). Again, we detected upregulation of CDK1 kinase activity as cells entered S phase (Fig. 3h). Collectively, these observations indicated that CDK1 might play a physiological role during G1/S transition.

To test whether CDK1 kinase activity is required during S-phase entry, we arrested CDC7$^{AID/AID}$/TIR1 ES cells in M phase with nocodazole, released the cells and monitored cell cycle progression (Fig. 3i, top). When cells reached G1 phase, we degraded CDC7 with

IAA and/or inhibited CDK1 (using the CDK1 inhibitor, Ro-3306) and continued cell culture in the presence of the compound(s). Consistent with the results described above, CDC7-degraded cells entered and progressed through S phase, although at a reduced pace (Fig 3i, third panel). Cells that underwent CDK1 inhibition also progressed through S phase (Fig. 3i, second panel). Notably, combined inhibition of CDC7 and CDK1 essentially blocked the entry of cells into S phase (Fig. 3i, bottom), and similar results were seen in *Cdk2* knockout ES cells (Extended Data Fig. 7h). Consistent with these findings, treatment of asynchronously growing ES cells with IAA plus a CDK1 inhibitor impeded the firing of DNA replication origins, as revealed by DNA combing (Fig. 3j).

Essentially identical results were obtained using CDK1$^{AS/AS}$ ES cells, which allow highly specific CDK1 inhibition with inhibitors of analogue-sensitive kinases. Again, the combined inhibition of CDK1 (with 3MB-PP1) and CDC7 (with the CDC7 inhibitor XL-413) in G1 phase strongly inhibited S-phase entry (Extended Data Fig. 7i, bottom) and impeded origin firing (Extended Data Fig. 7j), whereas single treatments had modest effects (Extended Data Fig. 7i, j). We also detected a similar requirement for CDC7 and CDK1 at the G1/S transition in human glioblastoma T98G cells (Extended Data Fig. 7k, l). Importantly, we verified that inhibition of CDK1 or CDC7, or both, did not impede the activity of endogenous CDK2 (Extended Data Fig. 8).
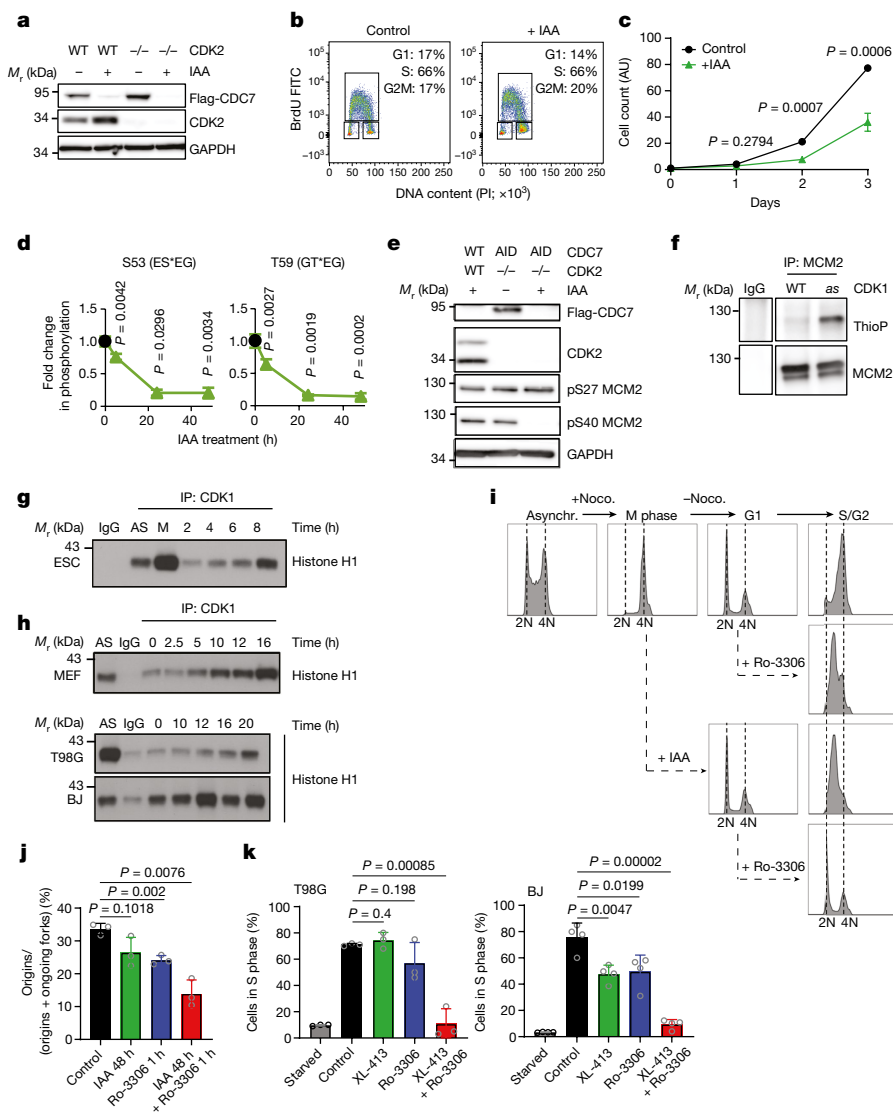
Fig. 3 | Analyses of CDK1 in S-phase entry. a, Immunoblotting of $Cdk2^{+/+}$ (WT) and $Cdk2$ knockout ($Cdk2^{-/-}$) CDC7$^{AID/AID}$/TIR1 ES cells treated with auxin (IAA). **b**, Flow cytometry of $Cdk2$ knockout/CDC7$^{AID/AID}$/TIR1 ES cells treated with IAA or vehicle (control). **c**, Growth curves of $Cdk2$ knockout/CDC7$^{AID/AID}$/TIR1 ES cells treated with IAA or vehicle. **d**, Quantification of MCM2 phosphorylation at known and predicted CDC7 phosphorylation sites in CDC7$^{AID/AID}$/TIR1 ES cells treated with IAA for 5, 24 and 48 h, using quantitative mass spectrometry. Black dots indicate phosphorylation levels at time 0. **e**, Immunoblots of $Cdk2^{+/+}$ (WT) and $Cdk2^{-/-}$ CDC7$^{AID/AID}$/TIR1 (AID) ES cells for CDC7-dependent (S40) and CDC7-independent (S27) MCM2 phosphoresidues. Cells were treated with IAA for 24 h. **f**, In-cell phosphorylation of MCM2 by CDK1. IgG, control immunoprecipitation from CDK1$^{AS/AS}$ cells. ThioP, thiophosphate. **g**, **h**, ES cells were released from mitosis (**g**), whereas MEFs, glioblastoma T98G and BJ foreskin fibroblasts were released from G0 (**h**). CDK1 was immunoprecipitated at the indicated time points and used for kinase reactions with histone H1 as the

substrate. AS, asynchronous cells; M, mitosis-arrested cells. IgG, control immunoprecipitation. **i**, Asynchronously growing CDC7$^{AID/AID}$/TIR1 ES cells (Asynchr.) were synchronized in mitosis by nocodazole (+Noco.; M phase) and released (−Noco). Following release, CDC7 degradation was induced through the addition of IAA to account for degradation time. Two hours later, when cells reached G1, they were treated with the CDK1 inhibitor Ro-3306. Cells were cultured in the presence of inhibitor(s), collected after 12 h (S/G2), stained with PI and analysed by flow cytometry. **j**, Fraction of new replication origins in CDC7$^{AID/AID}$/TIR1 ES cells treated with IAA for 48 h and/or Ro-3306 for the last 1 h, or with vehicle. **k**, T98G and BJ cells were arrested in G0 and released in the presence of the CDC7 inhibitor XL-413 and/or Ro-3306 or vehicle. Cells were pulsed with BrdU after 19 h and analysed by flow cytometry. For **c**, **d**, **j** and **k**, mean values are shown, with error bars representing the s.d. P values were determined by two-sided t-test. For **c**, **d**, **j** and **k**, $n = 3$ independent replicates; **a**, **b**, **e**–**i**, representative results (out of two) are shown.

We extended these findings using four types of human non-transformed cells and T98G cells that were arrested in G0 phase and then stimulated to re-enter the cell cycle. Again, inhibition of CDC7 or CDK1 alone had only modest effects on G1/S progression, whereas combined inhibition blocked entry into S phase (Fig. 3k and Extended Data Fig. 7m–o). We concluded that CDC7 and CDK1 play functionally redundant roles in triggering S-phase entry in different human and mouse cell types, both in cycling cells and in cells re-entering the cell cycle from quiescence, and at least one of these kinases must be present to allow DNA synthesis.

Live-cell imaging

To verify these findings at single-cell resolution, we performed combined live-cell and fixed-cell imaging of CDC7$^{AID/AID}$/TIR1 MEFs, human mammary epithelial MCF10A cells and primary human dermal fibroblasts. We live-imaged asynchronously growing cells in the presence of IAA or CDC7 inhibitors (human cells) or vehicle. Cells were also acutely treated with the CDK1 inhibitor Ro-3306, and we analysed cells that received CDK1 inhibitor in G1 phase (starting within the first 2 h after completion of mitosis). CDC7-inhibited or CDK1-inhibited cells entered
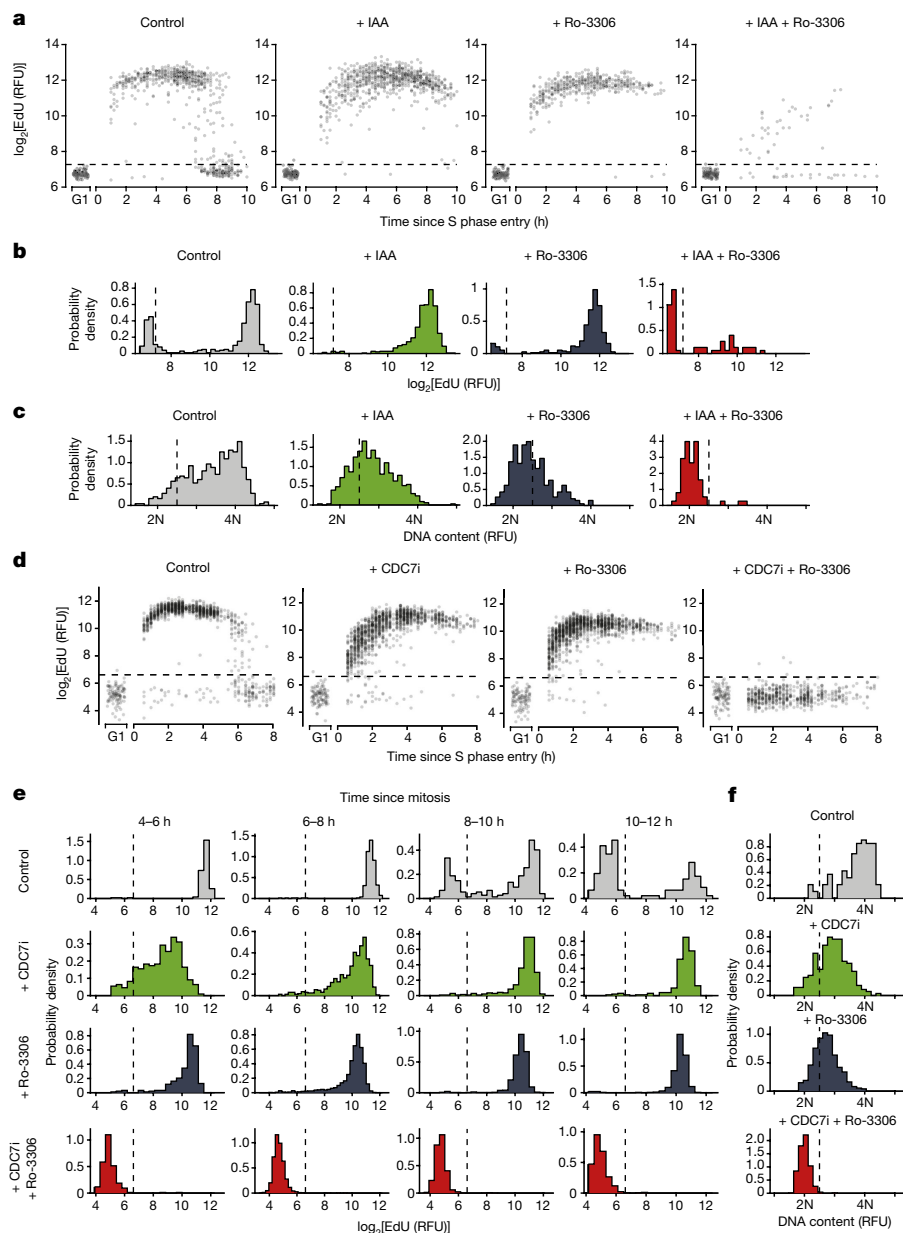
Fig. 4 | Live-cell imaging of Cdc7-depleted cells. a–c, Asynchronously growing immortalized CDC7[AID/AID]/TIR1 MEFs expressing FUCCI(CA) reporters were live-imaged in the presence of auxin (IAA) or vehicle for 4 h, and then the CDK1 inhibitor Ro-3306 was added. Cells treated with Ro-3306 starting at 0–2 h after mitotic exit (in G1 phase) were selected for analysis. **a**, EdU intensity at the indicated times after S-phase entry (recorded as Cdt1[(1–100)Cy(–)]drop), in cells treated as indicated. **b**,**c**, EdU (**b**) and Hoechst intensity (DNA content) (**c**) in cells 16–18 h after mitosis, treated as indicated. **d–f**, MCF10A cells expressing FUCCI(CA) reporters were live-imaged as in **a–c**. Cells were treated with vehicle, the CDC7 inhibitor TAK-931 (CDC7i), Ro-3306 or with both inhibitors. Cells treated with drug(s) starting at 0–2 h after mitotic exit were selected for analysis. **d**, EdU intensity at the indicated times after S phase start (Cdt1[(1–100)Cy(–)]drop) in cells treated as indicated. **e**, Intensity of EdU incorporation at the indicated times after completion of mitosis. **f**, Hoechst intensity (DNA content) in cells treated as above, 10–12 h after mitotic exit. Dashed horizontal lines (**a**, **d**), cut-off values for EdU-positive signal. Dashed vertical lines: **b**, **e**, cut-off values for EdU-positive signal; **c**, **f**, signal corresponding to >2N DNA significantly above 2N noise.

and progressed through S phase (as determined by EdU incorporation and Hoechst staining for DNA content), albeit at reduced speed. By contrast, combined inhibition of CDC7 and CDK1 in G1 phase essentially abrogated S-phase entry (almost no EdU incorporation) and arrested cells with 2N content, which indicated a complete G1/S block following CDC7 and CDK1 inhibition (Fig. 4 and Extended Data Fig. 9a–c).

We also used live-cell imaging to further dissect events at G1/S transition. We engineered CDC7[AID/AID]/TIR1 MEFs and human cells to express FUCCI(CA) cell cycle reporters[22] (Extended Data Fig. 9d). This dual fluorescent reporter system detects two important events at the G1/S boundary: APC/C inactivation (Gem[(1–110)]–mCherry reporter), which reflects commitment to S-phase entry, and the start of DNA replication (Cdt1[(1–100)Cy(–)]–mVenus reporter).

We live-imaged asynchronously growing CDC7[AID/AID]/TIR1 MEFs in the presence of IAA or vehicle, and acutely treated cells with the CDK1 inhibitor Ro-3306. We analysed cells that received the CDK1 inhibitor within the first 2 h after completion of mitosis (that is, in G1). In control cells, Gem[(1–110)]rise (corresponding to APC/C inactivation) occurred approximately 7.5 h after mitosis (Extended Data Fig. 9e). Gem[(1–110)]rise was followed immediately by Cdt1[(1–100)Cy(–)]drop (indicative of the start of DNA replication) (Extended Data Fig. 9f, g), which was accompanied by the onset of EdU incorporation (Fig. 4a, d). Inhibition of CDC7 or CDK1
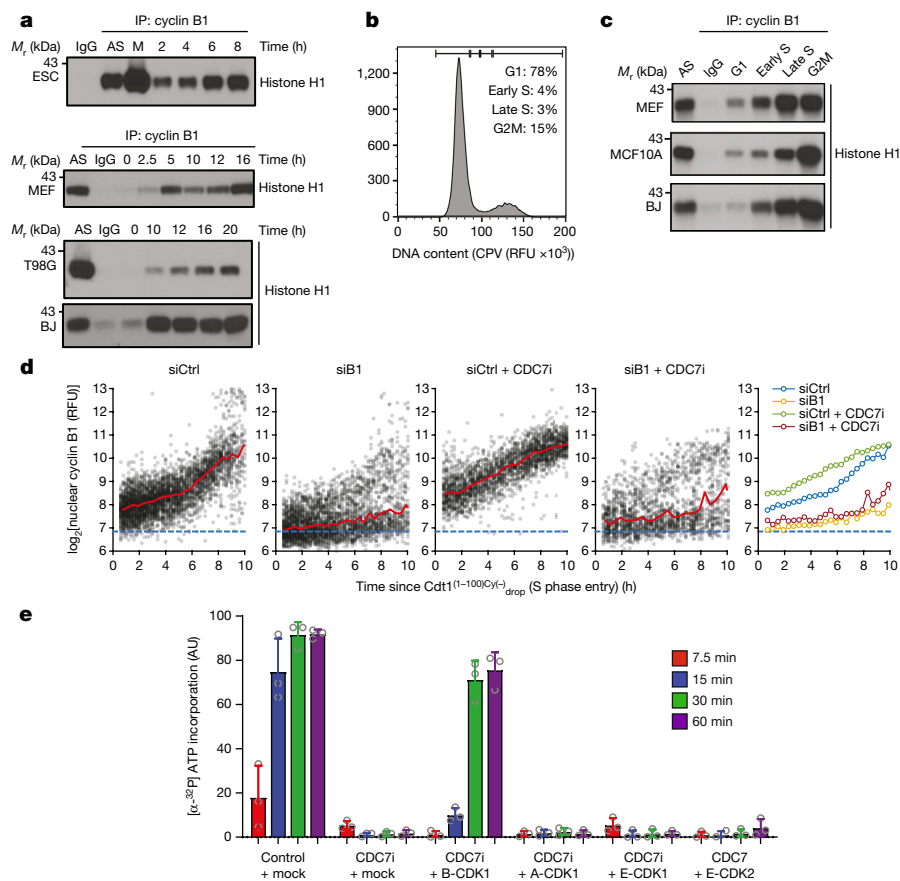
Fig. 5 | Analyses of CDK1–cyclin B at G1/S. a, ES cells were synchronized in M phase with nocodazole; MEFs, T98G and BJ cells were arrested in G0. Cells were released and collected at the indicated time points for cyclin B1 immunoprecipitation (IP) followed by kinase reactions with [γ^{32}P]-ATP and histone H1 as substrate. AS, asynchronous cells; M, M phase cells; IgG, control immunoprecipitation. **b**, Example of the gating strategy for flow sorting. BJ foreskin fibroblasts were stained with CytoPhase Violet (CPV) and sorted using gates indicated at the top. **c**, Cyclin B1 was immunoprecipitated from flow-sorted cells and subjected to kinase reactions as in **a**. **d**, MCF10A cells expressing Cdt1$^{(1–100)Cy(–)}$–mCherry reporter were stained with anti-cyclin B1 antibody. For antibody control, cells were transfected with anti-cyclin B1 (siB1) or control siRNA (siCtrl) 24 h before fixation. Shown is intensity of nuclear

cyclin B1 at the indicated time points after Cdt1$^{(1–100)Cy(–)}$$_{drop}$ (S-phase entry). Red lines, median values within bins every two time-points (24 min, 12 min interval); blue dashed lines, mean nuclear cyclin B1 signal in cells treated with siB1 (background level). Right, median intensity of nuclear cyclin B1 at indicated time points after S-phase entry in different treatment groups. CDC7i, cells treated with the CDC7 inhibitor TAK-931. **e**, Quantification of DNA-replication assays in *Xenopus* egg extracts (from Extended Data Fig. 12i). Extracts were treated with PHA-767491 (CDC7i) or DMSO (control), cyclin–CDK complexes were added and nascent strand DNA synthesis assessed at indicated time points. Bars, mean values, error bars, s.d., *n* = 3 independent replicates. For **a**, **b**, **c**, representative results (out of two) are shown.

alone or combined did not affect the timing of Gem$^{(1–110)}$$_{rise}$ (APC/C inactivation) (Extended Data Fig. 9e), which is consistent with the notion that CDC7 and CDK1 activity is not necessary for APC/C inactivation at G1/S. Cells treated with a CDC7 or CDK1 inhibitor alone exhibited only a minor delay in Cdt1$^{(1–100)Cy(–)}$$_{drop}$ (indicating S-phase entry; Extended Data Fig. 9h). By contrast, combined inhibition of CDC7 and CDK1 strongly delayed Cdt1$^{(1–100)Cy(–)}$$_{drop}$ (S-phase entry) relative to Gem$^{(1–110)}$$_{rise}$ (APC/C inactivation), with a large fraction of cells failing to enter S phase (Extended Data Fig. 9f, g). Notably, nearly all CDC7- and CDK1-inhibited cells (including those with Cdt1$^{(1–100)Cy(–)}$$_{drop}$) failed to incorporate EdU and did not increase their DNA content beyond 2N (Fig. 4), indicating a complete G1/S block following CDC7 and CDK1 inhibition.

We recapitulated these observations using asynchronously growing human cells (Extended Data Fig. 9i, j) and human cells that were rendered quiescent and then stimulated to re-enter the cell cycle (Extended Data Fig. 9k). In these cells, combined inhibition of CDC7 and CDK1 almost completely abrogated Cdt1$^{(1–100)Cy(–)}$$_{drop}$ (S-phase entry), whereas there was essentially no effect on Gem$^{(1–110)}$$_{rise}$ (APC/C inactivation) (Extended Data Fig. 9i–k). Treatment with either CDC7 or CDK1 inhibitor alone had little effect on these parameters.

Collectively, these findings demonstrate that combined inhibition of CDC7 and CDK1 prevents the onset of DNA synthesis in mouse and human cells.

Cyclin B–CDK1 at G1/S

Our results indicated that in addition to its well-established role in mitosis, CDK1 has an important function in triggering S-phase entry. This role is performed in a functionally redundant fashion with CDC7; hence inhibition of CDC7 renders CDK1 rate-limiting for S-phase entry.

During mitosis, CDK1 is activated by cyclin B, whereas CDK1 partners with cyclin A during late S phase[1]. CDK1 can also bind cyclin E in *Cdk2* knockout cells[23]. To determine which cyclin mediates the function of CDK1 during S-phase entry, we examined the association of CDK1 with cyclin A, cyclin B and cyclin E during G1/S phase progression in wild-type ES cells synchronized by mitotic block and release, and during cell cycle re-entry of wild-type MEFs and human cells. CDK1 was associated with cyclin B, but not with detectable cyclin E or cyclin A during G1/S progression both in cells exiting mitosis and in cells returning from quiescence (Extended Data Figs. 7e, g and 10a–d).

Article

These findings prompted us to analyse cyclin B-associated kinase activity during G1/S progression in ES cells (Fig. 5a, top, and Extended Data Fig. 7e), and during cell cycle re-entry of MEFs and human cells (Fig. 5a, middle and lower panels, and Extended Data Fig. 7g). We observed that CDK1–cyclin B kinase becomes activated as cells enter S phase, both in cycling cells and during cell cycle re-entry (Fig. 5a).

To evaluate the presence and activity of CDK1–cyclin B in cells under unperturbed conditions, we stained asynchronously growing MEFs and human BJ foreskin fibroblasts and MCF10A cells with cell-permeant DNA-binding dyes CytoPhase Violet or Hoechst-33342. We then flow-sorted cells from G1, early S, late S and G2/M fractions on the basis of DNA content (Fig. 5b), immunoprecipitated cyclin B and performed kinase and co-immunoprecipitation assays. CDK1–cyclin B complexes and cyclin B-associated kinase activity were observed in early S phase in all the three cell types analysed (Fig. 5c and Extended Data Fig. 10e–g).

Cyclin B is localized to the cytoplasm during interphase and it translocates to the nucleus when cells enter M phase. We asked whether lower levels of cyclin B might be present in the nuclei at the onset of S phase to take part in DNA replication. Combined live-cell imaging and immunofluorescence staining revealed clear upregulation of nuclear cyclin B1 levels in asynchronously growing cells entering S phase (Fig. 5d and Extended Data Fig. 10h, i). Notably, inhibition of CDC7 resulted in increased levels of cyclin B at the start of S phase, which indicated that this physiological mechanism is upregulated in the absence of CDC7 activity (Fig. 5d and Extended Data Fig. 10h, i). Moreover, combined live-cell imaging and immunofluorescence analysis revealed that CDK1 is present in cell nuclei across the cell cycle, including G1 and early S phase cells (Extended Data Figs. 11 and 12a–h).

Last, we used *Xenopus* egg extracts to test the ability of different cyclin–CDK combinations to drive S-phase entry in the absence of CDC7 activity. Consistent with previous results[24], treatment with the CDC7 inhibitor PHA-767491 greatly inhibited DNA replication in this cell-free system (Fig. 5e and Extended Data Fig. 12i). The addition of recombinant CDK1–cyclin B1, but not CDK1–cyclin A2, CDK1–cyclin E1 or CDK2–cyclin E1, restored DNA replication following CDC7 inhibition (Fig. 5e and Extended Data Fig. 12i). These results provide further support for our findings that CDK1–cyclin B can promote DNA replication initiation in the absence of CDC7 activity.

Discussion

We developed a new system that enables rapid, global and reversible degradation of a protein in vivo. This system represents a powerful tool to study essentially any protein in normal physiology and in any pathological condition. In the current work, we applied this technology to CDC7 kinase.

According to established models, CDC7 represents an essential kinase that is required for origin firing[10,15,24–33]. However, some previous observations have hinted that the requirement for CDC7 may not be absolute. In *Saccharomyces cerevisiae*, a recessive mutation in *mcm5* (also known as *cdc46*) bypassed the requirement for Cdc7 in cell division[34–36]. In fission yeast, proliferation of Hsk1(Cdc7)-null cells could be restored by the deletion of Mrc1 (a component of DNA replication forks) or Rif1 (refs. [37,38]). In *Xenopus* and in human cells, depletion of RIF1—a protein that recruits PP1 phosphatase to replication origins to dephosphorylate MCM proteins—rendered the phosphorylation of MCM proteins relatively insensitive to CDC7 inhibition[39]. A very early embryonic lethality of *Cdc7*^{−/−} mice could be overcome by knockout of p53, whereby *Cdc7*^{−/−} *p53*^{−/−} animals survived until embryonic day 8, a stage at which several major organs have been developed[33].

In the current study, we observed that acute shutdown of CDC7 did not arrest the proliferation of cells grown in vitro and in tissues of live mice, and that some mouse cell types physiologically proliferated without detectable CDC7. We conclude that CDC7 is not uniformly required for mammalian cell proliferation.

Phosphorylation of MCM proteins is thought to represent the essential function of CDC7 (refs. [4–8]). Our analyses revealed that shutdown of CDC7 strongly decreased the phosphorylation of some, but not all, MCM phosphoresidues. We also found that CDK1 can phosphorylate MCM proteins on CDC7-independent sites. These observations suggest that CDC7 and CDK1 collaborate and independently contribute to G1/S transition by phosphorylating distinct MCM residues, and that phosphorylation of a subset of MCM sites (either by CDC7 or CDK1) is sufficient to drive S-phase entry. By contrast, CDK2 does not seem to be essential in this process.

Notably, we found that during S-phase entry, CDK1 associates with cyclin B, and these CDK1–cyclin B complexes are catalytically active. These results are in line with some previously published observations. In *Xenopus* egg extracts, Cdk1–cyclin B can promote DNA replication when directed to the nucleus and activated[40]. Also, in nucleus-free *Xenopus* egg extracts, Cdk1–cyclin B efficiently supported DNA replication[41]. Cdk1–cyclin B was shown to phosphorylate Mcm2 and Mcm4 in vitro, and this augmented subsequent phosphorylation by Cdc7 (ref. [21]). Although cyclin B translocates to the nucleus at the onset of mitosis, nuclear expression of cyclin B1 during G1 phase was documented in cancer cell lines[42,43], in agreement with our findings.

A recent study using human immortalized retinal pigment epithelial cells expressing analogue-sensitive CDC7 revealed that inhibition of CDC7 blocked cell proliferation[44]. Importantly, in that study, CDC7 was not required for firing of early replication origins. Firing of late origins was blocked owing to stalled replication forks and ATR-dependent S phase checkpoint[44]. It is likely that under suboptimal conditions that cause replicative stress and stalling of DNA forks, CDC7 becomes rate-limiting in overcoming the stalled forks. Also, inactivation of CDC7 in murine ES cells was reported to cause stalled replication forks, induction of p53, activation of G2/M checkpoint, inhibition of CDK1 kinase and ultimately p53-dependent cell death[33]. It is probable that this phenotype reflects a stress response of cells acutely transduced with Cre-encoding adenoviruses. Moreover, several other studies have implicated CDC7 function under replicative stress[45–47]. Hence, CDC7 may have mechanistically at least two distinct functions: a non-essential role in DNA replication and another major function in counteracting replicative stress.

Cancer cells display higher level of replicative stress and hence may be particularly sensitive to CDC7 inhibition. CDC7 is upregulated in cancer cells, and overexpression of CDC7 correlates with poor clinical prognosis[10,16]. Depletion of CDC7 or inhibition of CDC7 kinase was shown to trigger apoptosis, or senescence, predominantly in p53-mutant cancer cells[10,15,16,32,48]. These results—together with our findings that CDC7 is largely dispensable in vivo—raise the possibility that CDC7 inhibition might represent an attractive therapeutic strategy, in particular against p53-mutant tumours.

Online content

Any methods, additional references, Nature Research reporting summaries, source data, extended data, supplementary information, acknowledgements, peer review information; details of author contributions and competing interests; and statements of data and code availability are available at https://doi.org/10.1038/s41586-022-04698-x.

1. Asghar, U., Witkiewicz, A. K., Turner, N. C. & Knudsen, E. S. The history and future of targeting cyclin-dependent kinases in cancer therapy. *Nat. Rev. Drug. Discov.* **14**, 130–146 (2015).
2. Chuang, L. C. et al. Phosphorylation of Mcm2 by Cdc7 promotes pre-replication complex assembly during cell-cycle re-entry. *Mol. Cell* **35**, 206–216 (2009).
3. Heller, R. C. et al. Eukaryotic origin-dependent DNA replication in vitro reveals sequential action of DDK and S-CDK kinases. *Cell* **146**, 80–91 (2011).
4. Lei, M. et al. Mcm2 is a target of regulation by Cdc7–Dbf4 during the initiation of DNA synthesis. *Genes Dev.* **11**, 3365–3374 (1997).
5. Sheu, Y. J. & Stillman, B. Cdc7–Dbf4 phosphorylates MCM proteins via a docking site-mediated mechanism to promote S phase progression. *Mol. Cell* **24**, 101–113 (2006).
6. Sheu, Y. J. & Stillman, B. The Dbf4–Cdc7 kinase promotes S phase by alleviating an inhibitory activity in Mcm4. *Nature* **463**, 113–117 (2010).

7. Tsuji, T., Ficarro, S. B. & Jiang, W. Essential role of phosphorylation of MCM2 by Cdc7/Dbf4 in the initiation of DNA replication in mammalian cells. *Mol. Biol. Cell* **17**, 4459–4472 (2006).
8. Yeeles, J. T., Deegan, T. D., Janska, A., Early, A. & Diffley, J. F. Regulated eukaryotic DNA replication origin firing with purified proteins. *Nature* **519**, 431–435 (2015).
9. Douglas, M. E., Ali, F. A., Costa, A. & Diffley, J. F. X. The mechanism of eukaryotic CMG helicase activation. *Nature* **555**, 265–268 (2018).
10. Bonte, D. et al. Cdc7–Dbf4 kinase overexpression in multiple cancers and tumor cell lines is correlated with p53 inactivation. *Neoplasia* **10**, 920–931 (2008).
11. Witucki, L. A. et al. Mutant tyrosine kinases with unnatural nucleotide specificity retain the structure and phospho-acceptor specificity of the wild-type enzyme. *Chem. Biol.* **9**, 25–33 (2002).
12. Michowski, W. et al. Cdk1 controls global epigenetic landscape in embryonic stem cells. *Mol. Cell* **78**, 459–476.e13 (2020).
13. Santamaria, D. et al. Cdk1 is sufficient to drive the mammalian cell-cycle. *Nature* **448**, 811–815 (2007).
14. Nishimura, K., Fukagawa, T., Takisawa, H., Kakimoto, T. & Kanemaki, M. An auxin-based degron system for the rapid depletion of proteins in nonplant cells. *Nat. Methods* **6**, 917–922 (2009).
15. Montagnoli, A. et al. Cdc7 inhibition reveals a p53-dependent replication checkpoint that is defective in cancer cells. *Cancer Res.* **64**, 7110–7116 (2004).
16. Rodriguez-Acebes, S. et al. Targeting DNA replication before it starts: Cdc7 as a therapeutic target in p53-mutant breast cancers. *Am. J. Pathol.* **177**, 2034–2045 (2010).
17. Berthet, C., Aleem, E., Coppola, V., Tessarollo, L. & Kaldis, P. Cdk2 knockout mice are viable. *Curr. Biol.* **13**, 1775–1785 (2003).
18. Ortega, S. et al. Cyclin-dependent kinase 2 is essential for meiosis but not for mitotic cell division in mice. *Nat. Genet.* **35**, 25–31 (2003).
19. Komamura-Kohno, Y. et al. Site-specific phosphorylation of MCM4 during the cell-cycle in mammalian cells. *FEBS J.* **273**, 1224–1239 (2006).
20. Lin, D. I., Aggarwal, P. & Diehl, J. A. Phosphorylation of MCM3 on Ser-112 regulates its incorporation into the MCM2-7 complex. *Proc. Natl Acad. Sci. USA* **105**, 8079–8084 (2008).
21. Masai, H. et al. Human Cdc7-related kinase complex. In vitro phosphorylation of MCM by concerted actions of Cdks and Cdc7 and that of a criticial threonine residue of Cdc7 by Cdks. *J. Biol. Chem.* **275**, 29042–29052 (2000).
22. Sakaue-Sawano, A. et al. Genetically encoded tools for optical dissection of the mammalian cell-cycle. *Mol. Cell* **68**, 626–640.e5 (2017).
23. Aleem, E., Kiyokawa, H. & Kaldis, P. Cdc2–cyclin E complexes regulate the G1/S phase transition. *Nat. Cell Biol.* **7**, 831–836 (2005).
24. Takahashi, T. S. & Walter, J. C. Cdc7–Drf1 is a developmentally regulated protein kinase required for the initiation of vertebrate DNA replication. *Genes Dev.* **19**, 2295–2300 (2005).
25. Bahman, M., Buck, V., White, A. & Rosamond, J. Characterisation of the *CDC7* gene product of *Saccharomyces cerevisiae* as a protein kinase needed for the initiation of mitotic DNA synthesis. *Biochim. Biophys. Acta* **951**, 335–343 (1988).
26. Bousset, K. & Diffley, J. F. The Cdc7 protein kinase is required for origin firing during S phase. *Genes Dev.* **12**, 480–490 (1998).
27. Donaldson, A. D., Fangman, W. L. & Brewer, B. J. Cdc7 is required throughout the yeast S phase to activate replication origins. *Genes Dev.* **12**, 491–501 (1998).
28. Masai, H., Miyake, T. & Arai, K. *hsk1⁺*, a *Schizosaccharomyces pombe* gene related to *Saccharomyces cerevisiae* CDC7, is required for chromosomal replication. *EMBO J.* **14**, 3094–3104 (1995).
29. Roberts, B. T., Ying, C. Y., Gautier, J. & Maller, J. L. DNA replication in vertebrates requires a homolog of the Cdc7 protein kinase. *Proc. Natl Acad. Sci. USA* **96**, 2800–2804 (1999).
30. Silva, T., Bradley, R. H., Gao, Y. & Coue, M. *Xenopus* CDC7/DRF1 complex is required for the initiation of DNA replication. *J. Biol. Chem.* **281**, 11569–11576 (2006).
31. Jiang, W., McDonald, D., Hope, T. J. & Hunter, T. Mammalian Cdc7–Dbf4 protein kinase complex is essential for initiation of DNA replication. *EMBO J.* **18**, 5703–5713 (1999).
32. Montagnoli, A. et al. A Cdc7 kinase inhibitor restricts initiation of DNA replication and has antitumor activity. *Nat. Chem. Biol.* **4**, 357–365 (2008).
33. Kim, J. M. et al. Inactivation of Cdc7 kinase in mouse ES cells results in S-phase arrest and p53-dependent cell death. *EMBO J.* **21**, 2168–2179 (2002).
34. Hardy, C. F., Dryga, O., Seematter, S., Pahl, P. M. & Sclafani, R. A. mcm5/cdc46-bob1 bypasses the requirement for the S phase activator Cdc7p. *Proc. Natl Acad. Sci. USA* **94**, 3151–3155 (1997).
35. Hoang, M. L. et al. Structural changes in Mcm5 protein bypass Cdc7–Dbf4 function and reduce replication origin efficiency in *Saccharomyces cerevisiae*. *Mol. Cell. Biol.* **27**, 7594–7602 (2007).
36. Jackson, A. L., Pahl, P. M., Harrison, K., Rosamond, J. & Sclafani, R. A. Cell-cycle regulation of the yeast Cdc7 protein kinase by association with the Dbf4 protein. *Mol. Cell. Biol.* **13**, 2899–2908 (1993).
37. Hayano, M. et al. Rif1 is a global regulator of timing of replication origin firing in fission yeast. *Genes Dev.* **26**, 137–150 (2012).
38. Matsumoto, S., Hayano, M., Kanoh, Y. & Masai, H. Multiple pathways can bypass the essential role of fission yeast Hsk1 kinase in DNA replication initiation. *J. Cell Biol.* **195**, 387–401 (2011).
39. Alver, R. C., Chadha, G. S., Gillespie, P. J. & Blow, J. J. Reversal of DDK-mediated MCM phosphorylation by Rif1–PP1 regulates replication initiation and replisome stability independently of ATR/Chk1. *Cell Rep.* **18**, 2508–2520 (2017).
40. Moore, J. D., Kirk, J. A. & Hunt, T. Unmasking the S-phase-promoting potential of cyclin B1. *Science* **300**, 987–990 (2003).
41. Prokhorova, T. A., Mowrer, K., Gilbert, C. H. & Walter, J. C. DNA replication of mitotic chromatin in *Xenopus* egg extracts. *Proc. Natl Acad. Sci. USA* **100**, 13241–13246 (2003).
42. David-Pfeuty, T. & Nouvian-Dooghe, Y. Human cyclin B1 is targeted to the nucleus in G1 phase prior to its accumulation in the cytoplasm. *Oncogene* **13**, 1447–1460 (1996).
43. Shen, M. et al. Detection of cyclin B1 expression in G₁-phase cancer cell lines and cancer tissues by postsorting western blot analysis. *Cancer Res.* **64**, 1607–1610 (2004).
44. Jones, M. J. K. et al. Human DDK rescues stalled forks and counteracts checkpoint inhibition at unfired origins to complete DNA replication. *Mol. Cell* **81**, 426–441.e8 (2021).
45. Yang, C. C., Kato, H., Shindo, M. & Masai, H. Cdc7 activates replication checkpoint by phosphorylating the Chk1-binding domain of Claspin in human cells. *eLife* **8**, e50796 (2019).
46. Yamada, M. et al. ATR–Chk1–APC/CCdh1-dependent stabilization of Cdc7–ASK (Dbf4) kinase is required for DNA lesion bypass under replication stress. *Genes Dev.* **27**, 2459–2472 (2013).
47. Sasi, N. K. et al. DDK has a primary role in processing stalled replication forks to initiate downstream checkpoint signaling. *Neoplasia* **20**, 985–995 (2018).
48. Wang, C. et al. Inducing and exploiting vulnerabilities for the treatment of liver cancer. *Nature* **574**, 268–272 (2019).

Article

Extended Data Fig. 1 | Gene-targeting to generate mutant Cdc7 alleles.
a, Verification that analog-sensitive (*as*) Cdc7, but not wild-type Cdc7 can be potently inhibited by 1NM-PP1. 293T cells were transfected with constructs encoding Flag-tagged wild-type (wt) or *as* Cdc7. Cells were treated with DMSO (Vehicle) or 1NM-PP1, Cdc7 was immunoprecipitated using an anti-Flag antibody and subjected to kinase reactions with [γ^{32}P]-ATP and Mcm2 as a substrate. Immunoprecipitates were also immunoblotted with an anti-Flag antibody. **b**, Gene-targeting strategy to generate the *Cdc7^{AS}* allele. *Cdc7* exons are numbered, coding exons are in grey. M128G, *as* substitution; Puro, puromycin resistance cassette; 4x polyA, polyadenylation signal; red triangles, *LoxP* sites. **c**, Growth curves of Cdk1$^{AS/AS}$ ESC cultured in the presence of vehicle (Control) or 3MB-PP1. **d**, Cdk1$^{AS/AS}$ ESC treated as in **c** for 24h were stained with propidium iodide and analyzed by flow cytometry. Note that Cdk1-inhibited cells arrested in G2 phase, as expected. **e**, The principle of auxin-inducible degradation system. A plant hormone auxin recruits proteins containing the auxin-inducible degron (AID) domain to E3 ubiquitin ligase Cul1–Rbx1–Skp1–Tir1 (SCF^{Tir1}) for polyubiquitination and subsequent degradation by the proteasome. **f**, Gene-targeting strategy to knock-in the AID domain and 3xFlag-tag into the *Cdc7* gene in ESC. **g**, Immunoblot analysis of wild-type (wt) and Cdc7$^{AID/AID}$/Tir1 (AID) ESC for expression of Flag-tagged Cdc7. **h**, Gene-targeting strategy to knock-in the Myc-tagged *Tir1* gene into *Rosa 26* locus. **i**, Immunoblot analysis of wild-type (wt) and Tir1 knock-in ESC for expression of Myc-tagged Tir1. Gapdh was used as loading control. **j**, To verify the absence of truncated, untagged Cdc7 species in Cdc7$^{AID/AID}$/Tir1 ESC, we prepared whole cell lysates (WCL) from these cells (lane 2), and probed immunoblots with an anti-Cdc7 antibody. In addition, we immunodepleted tagged Cdc7 from WCL using an anti-Flag antibody (IP-Flag) and probed immunoprecipitates (IP, lane 3) and supernatants (Sup, lane 4) with an anti-Cdc7 antibody. WCL from wild-type ESC were also immunoblotted (lane 1). We did not detect the presence of truncated Cdc7. **k**, To further exclude the presence of truncated Cdc7, we resolved WCL from Cdc7$^{AID/AID}$/Tir1 ESC on an SDS-PAGE gel, cut the gel into smaller fragments corresponding to different protein sizes and evaluated the presence of Cdc7 peptides in these fractions by mass spectrometry. We detected the presence of Cdc7 only in the fraction corresponding to the full-length protein. **l**, Gene-targeting strategy to generate Cdc7^{Flox} allele in ESC. Red triangles, *LoxP* sites. **c**, n=3 independent replicates; **a, d, g, i, j** show representative results (out of 2); **c**, *p*-values determined by two-sided t-test; error bars, SD.

a

b


c

d

e
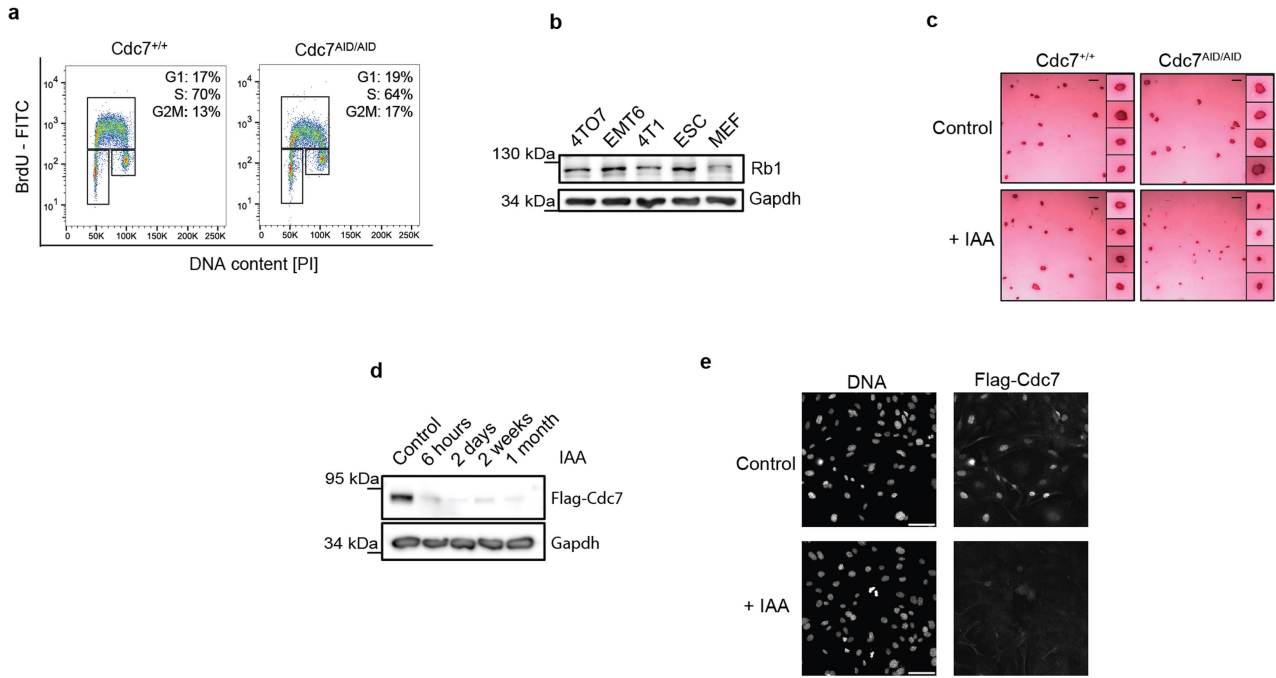
Extended Data Fig. 2 | Analyses of Cdc7^AID/AID cells. a, wild-type (Cdc7$^{+/+}$) and Cdc7$^{AID/AID}$/Tir1 ESC were cultured without auxin. Cells were pulsed with BrdU, stained with an anti-BrdU antibody and propidium iodide and analyzed by flow cytometry. Note normal cell cycle profile of Cdc7$^{AID/AID}$/Tir1 ESC in the absence of auxin, as expected. **b,** Immunoblot analysis to demonstrate expression of the retinoblastoma protein, Rb1, in wild-type ESC. Whole cell lysates from MEFs and mouse breast cancer cell lines (4TO7, EMT6, 4T1) were immunoblotted for control. **c,** Cdc7$^{+/+}$ and Cdc7$^{AID/AID}$/Tir1 ESC were cultured on feeders with auxin (IAA) or vehicle (Control) for 72 h and stained for alkaline phosphatase, a marker of undifferentiated pluripotent stem cells. Scale bar, 500 μm. Inserts, higher magnification of colonies. Inhibition of Cdc7 did not decrease alkaline phosphatase staining, suggesting that Cdc7 is not required to maintain pluripotency. **d,** Cdc7 protein levels in Cdc7$^{AID/AID}$/Tir1 ESC cultured with auxin for the indicated times. Immunoblots of whole cell lysates were probed with an anti-Flag antibody to detect Flag-tagged endogenous Cdc7. Efficient degradation of Cdc7 was maintained after 1 month of continuous culture with auxin. **e,** Immunostaining of Cdc7$^{AID/AID}$/Tir1 MEFs for expression of Cdc7. Cells were cultured with vehicle or auxin for 4 h, and stained with an anti-Flag antibody. Nuclei were counterstained with Hoechst. Note the loss Cdc7 staining after addition of auxin. See Fig. 1k for quantification. **a–e,** representative results (out of 2).
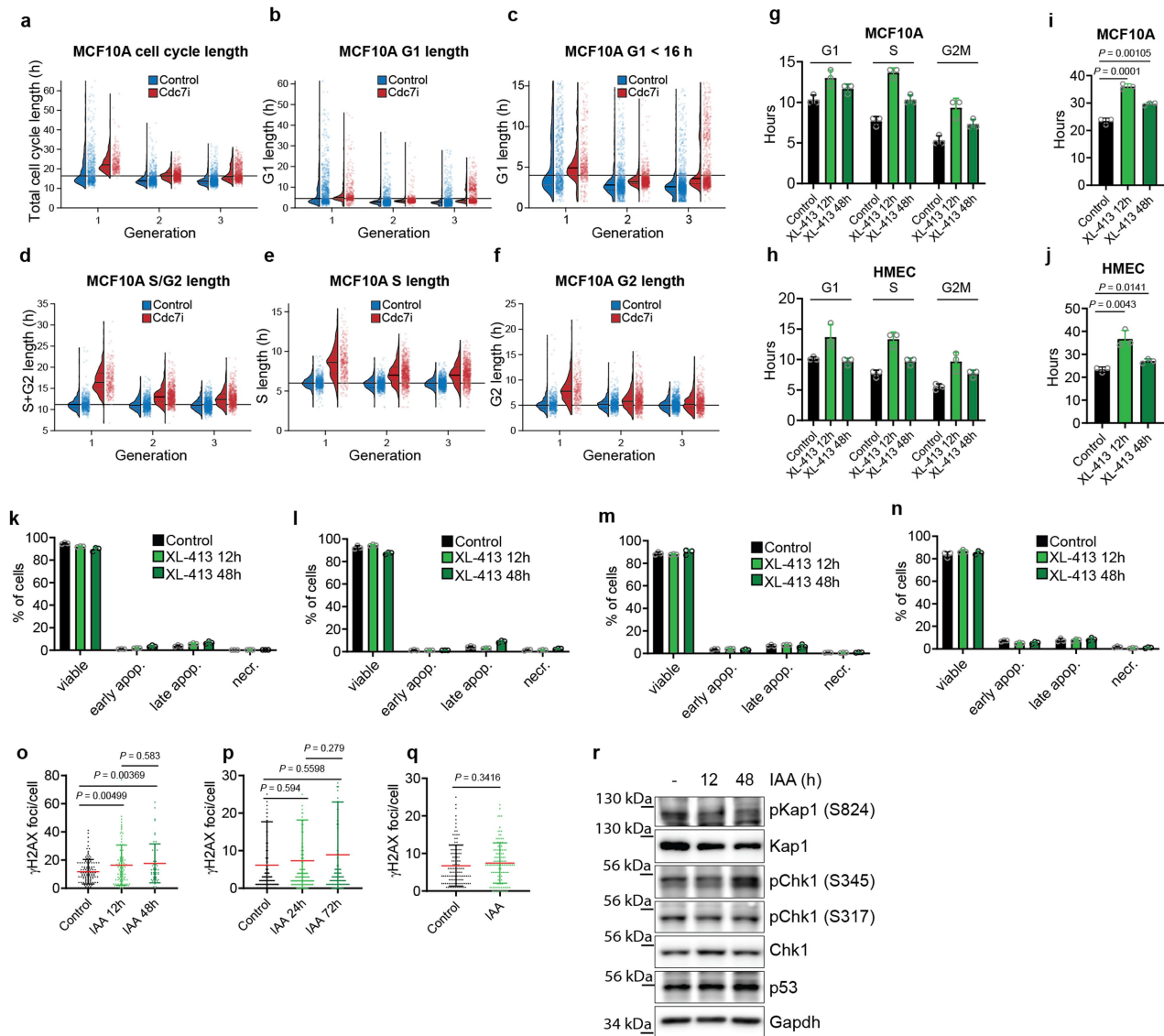
Extended Data Fig. 3 | Analyses of CDC7-inhibited cells. a–f, Long-term live-cell imaging. MCF10A cells expressing Gem[(1–110)]-mVenus and Cdt1[(1-100)Cy(-)]-mCherry FUCCI(CA) reporters were cultured and imaged for a total of 77 h. 8 h after imaging start, CDC7 inhibitor, TAK-931, was added to the culture medium, and cells were imaged for an additional 69 h. Shown are parameters for the first three cell cycles after addition of TAK-931 (generations 1–3, selecting cells which received TAK-931 0–2 h after mitosis). **a**, Total cell cycle length (time between two mitoses). **b**, G1 length (time between mitosis and Cdt1[(1-100)Cy(-)]$_{drop}$ [S phase start]). **c**, Shown is the subset of G1 cells from **b**, with G1 phase lasting less than 16 h. **d**, S/G2 length (time from Cdt1[(1-100)Cy(-)]$_{drop}$ [S phase start]) to subsequent mitosis. **e**, S phase length (time from Cdt1[(1-100)Cy(-)]$_{drop}$ [S phase start] to Cdt1[(1-100)Cy(-)]$_{rise}$ [S phase end]). **f**, G2 length (time from Cdt1[(1-100)Cy(-)]$_{rise}$ [S phase end]) to subsequent mitosis. In **a–f**, dots show values for individual cells; thin horizonal lines, median values; dotted lines above and below median, inter-quartile range; long horizonal lines, median values from control cells in generation 1. **g, h**, The length of G1, S and G2/M as determined by pulse-chase analysis in MCF10A (**g**) and HMEC human mammary epithelial cells (**h**) treated for the indicated times with CDC7 inhibitor, XL-413. Control, the length of cell cycle phases in untreated cells. **i, j**, Doubling times of MCF10A (**i**) and HMEC

cells (**j**) treated for the indicated times with XL-413, determined by pulse-chase analysis. Control, untreated cells. **k–n**, Human BJ foreskin fibroblasts (**k**), HMEC (**l**), human primary dermal fibroblasts (**m**), and MCF10A cells (**n**) were treated for the indicated times with XL-413, stained with Annexin V and propidium iodide (PI) and analyzed by flow cytometry. Shown are percentages of viable (Annexin V⁻/PI⁻), early apoptotic (Annexin V⁺/PI⁻), late apoptotic (Annexin V⁺/PI⁺) and necrotic (Annexin V⁻/PI⁺) cells. Control, untreated cells. **o, p**, Mean numbers of γH2AX foci/cell in Cdc7[AID/AID]/Tir1 ESC (**o**) and MEFs (**p**) cultured for the indicates times with auxin (IAA). Control, untreated cells. **q**, similar analysis for Cdc7[AID/AID]/Tir1 ESC cultured with auxin for 7 weeks. **r**, Cdc7[AID/AID]/Tir1 MEFs were treated with vehicle (−) or auxin for the indicated times. Lysates were immunoblotted with antibodies recognizing Chk1, p53, Kap1 (Trim28), phospho-Kap1 (serine 824), phospho-Chk1 (serine 317) and phospho-Chk1 (serine 345). Gapdh was used as loading control. **g–q**, show mean values; **i, j, o–q**, p-values determined by two-sided t-test; error bars, SD. **g–n**, n=3 independent replicates; **a–f**, n=2 independent replicates, **o–q**, data of n > 60 cells from at least 5 independent fields per experimental condition, **r**, representative results (out of 2).
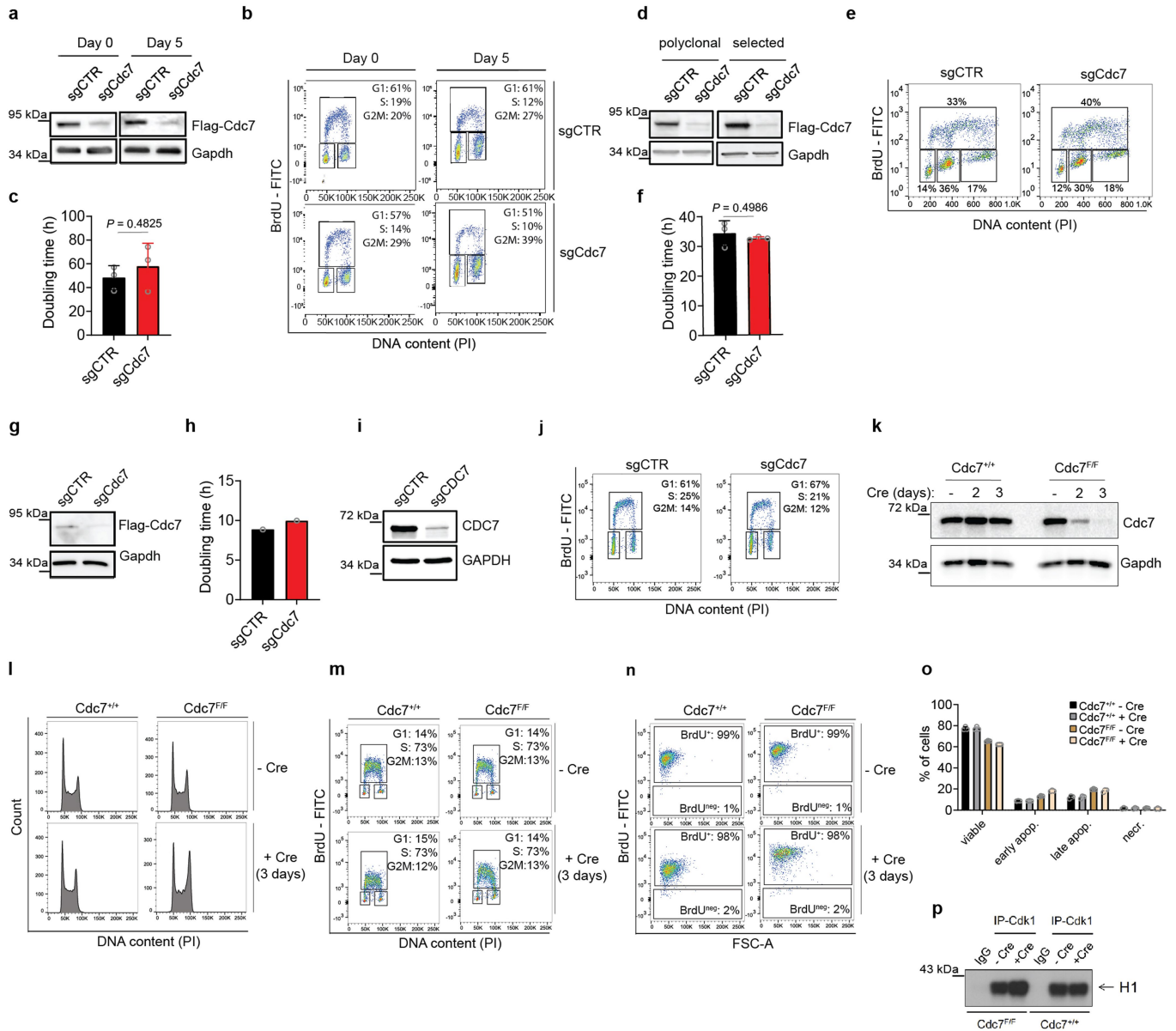
Extended Data Fig. 4 | Knockout of Cdc7. a-c, CRISPR/Cas9-mediated knockout of Cdc7 in primary mouse fibroblasts (MEFs). Cdc7[AID/AID]/Tir1 MEFs were transduced with viruses encoding control sgRNA (sgCTR) or anti-Cdc7 sgRNA (sgCdc7). **a**, Whole cell lysates were immunoblotted and probed with an anti-Flag antibody to detect Flag-tagged endogenous Cdc7. Day 0, cells at the end of selection; Day 5, cells after 5 days of culture. **b**, Cell cycle analysis of cells from **a**. Cells were pulsed with BrdU, stained with an anti-BrdU antibody and propidium iodide and analyzed by flow cytometry. **c**, Doubling times. **d–f**, CRISPR/Cas9-mediated knockout of Cdc7 in MEFs immortalized by dominant-negative p53. **d**, Immunoblotting as in **a**. Polyclonal, total polyclonal cell population after transduction with sgRNAs; selected, further purified population containing over 90% of Cdc7 frame-shift alleles. **e**, cell cycle analysis (polyclonal population), **f**, doubling times (polyclonal population). **g, h** CRISPR/Cas9-mediated knockout of Cdc7 in keratinocytes; **g**, immunoblotting, **h**, doubling time. **i–j**, CRISPR/Cas9-mediated knockout of CDC7 in human BJ foreskin fibroblasts. **i**, Immunoblotting with anti-CDC7 antibody, **j**, Cell cycle analysis. **k–p**, Acute ablation of Cdc7 in ESC. Cdc7[Flox/Flox] (Cdc7[F/F]) and Cdc7^{+/+} ESC were engineered to stably express dominant-negative p53 (to prevent p53-dependent cell death upon shutdown of Cdc7[33]). Cells were

transduced with lentiviruses encoding Cre-recombinase, or mock transduced. **k**, Cells were harvested at days 2 and 3, and extracts immunoblotted with an anti-Cdc7 antibody. **l, m**, at day 3, cells were stained with propidium iodide (**l**), or pulsed with BrdU and stained with propidium iodide and an anti-BrdU antibody (**m**) and analyzed by flow cytometry. **n**, Cells were cultured in the presence of BrdU for 15 h, stained with an anti-BrdU antibody and the percentage of BrdU^{+} cells was evaluated by flow cytometry. Note that 98% of Cdc7-deleted cells (and the same fraction of Cdc7^{+/+} cells) incorporated BrdU, indicating active DNA synthesis. FSC, forward scatter. **o**, Cells were stained with Annexin V and propidium iodide (PI) and analyzed by flow cytometry. Shown are percentages of viable (Annexin V[−]/PI[−]), early apoptotic (Annexin V[+]/PI[−]), late apoptotic (Annexin V[+]/PI[+]) and necrotic (Annexin V[−]/PI^{+}) cells. **p**, Cdk1 was immunoprecipitated (IP-Cdk1) from cells and used for kinase reactions with [γ32P]-ATP and histone H1 as a substrate. IgG, control immunoprecipitation with IgG. Note that ablation of Cdc7 resulted in modestly elevated levels of Cdk1 kinase - like an acute degradation of Cdc7 in Cdc7[AID/AID]/Tir1 ESC (Extended Data Fig. 7b). Gapdh was used as loading control. **c, f, o**, show means; *p*-values by two-sided t-test; error bars, SD; n = 3 independent replicates; other panels show representative results (out of 2).
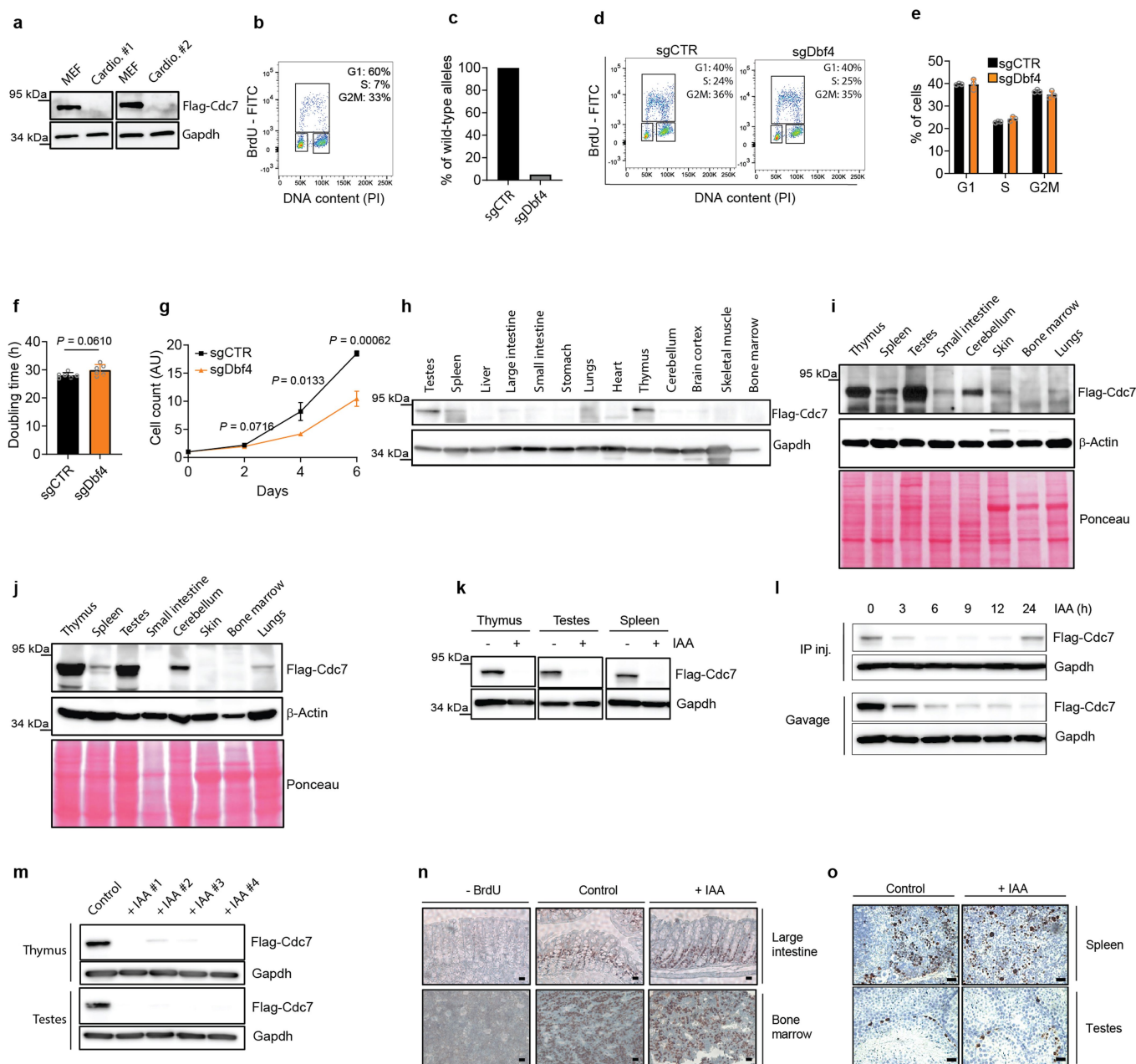
Extended Data Fig. 5 | Studies of Cdc7-Dbf4 in cells, and *in vivo* analyses using Cdc7^AID/AID/Tir1 mice. a, Analysis of cultured cardiomyocytes isolated from two independent litters of Cdc7^AID/AID/Tir1 embryos (Cardio. #1 and #2) for expression of Cdc7. Whole cell lysates were immunoblotted and probed with an anti-Flag antibody to detect Flag-tagged endogenous Cdc7. MEFs served as a positive control. Note that cardiomyocytes do not express appreciable levels of Cdc7, despite active proliferation. **b**, Cell cycle analysis. Cells were pulsed with BrdU, stained with an anti-BrdU antibody and propidium iodide and analyzed by flow cytometry. **c–g**, CRISPR/Cas9-mediated knockout of Dbf4 in MEFs immortalized by dominant-negative p53. **c**, Results of DNA sequencing of the *Dbf4* alleles in cells transduced with viruses encoding control sgRNA (sgCTR) or anti-Dbf4 sgRNA (sgDbf4). Shown is percentage of wild-type Dbf4 alleles in cell populations. **d**, Cell cycle analysis as in **b**. **e**, Distribution of cell cycle phases (from **d**). **f**, Doubling times; **g**, growth curves. **h–o**, *In vivo* analyses using Cdc7^AID/AID/Tir1 mice. **h, i**, Analysis of Cdc7 protein levels in the indicated organs of Cdc7^AID/AID/Tir1 mice. Lysates were immunoblotted and probed with an anti-Flag antibody to detect Flag-tagged endogenous Cdc7. In **i**, the immunoblot was overexposed to illustrate undetectable levels of Cdc7 in bone marrow. Note that except for testes and thymi, Cdc7 is expressed at very low levels. **j**, A similar analysis as in **h**, using organs from Cdc7^AID/AID Tir1-negative mice. **k**, The levels of Cdc7 protein in the indicated mouse organs after treatment of the animals with auxin for 12 h. **l**, This panel illustrates the efficiency of two routes of auxin administration: a single intraperitoneal injection (IP inj.) or a single oral gavage (Gavage). Mice received auxin via the indicated routes and thymi were collected at the indicated time-points for immunoblot analysis. Each of these routes resulted in an efficient Cdc7 degradation that lasted approximately 12 h. **m**, The levels of Cdc7 protein in thymi and testes of four Cdc7^AID/AID/Tir1 mice (#1 to #4) treated with auxin for 8 days. Control, a mouse treated with vehicle for 8 days. **n**, After 8 days of auxin treatment, Cdc7^AID/AID/Tir1 mice were injected with BrdU and sections stained with an anti-BrdU antibody. Control, a mouse treated for 8 days with vehicle, − BrdU, staining of sections from a mouse not injected with BrdU. Scale bars, 100 μm. **o**, Sections of organs from Cdc7^AID/AID/Tir1 mice treated with auxin for 4 days were stained with an anti-Ki67 antibody (to detect proliferating cells). Scale bars, 100 μm. Gapdh and β-actin were used as loading controls; **i, j**, show Ponceau S-stained membrane. **e–g** show means; *p*-values by two-sided t-test; error bars, SD. **e**, n = 3; **f, g**, n = 6, **a–d, h–l** representative results (out of 2); **m**, n=4 **n, o**, representative images (of at least 5 independent fields).
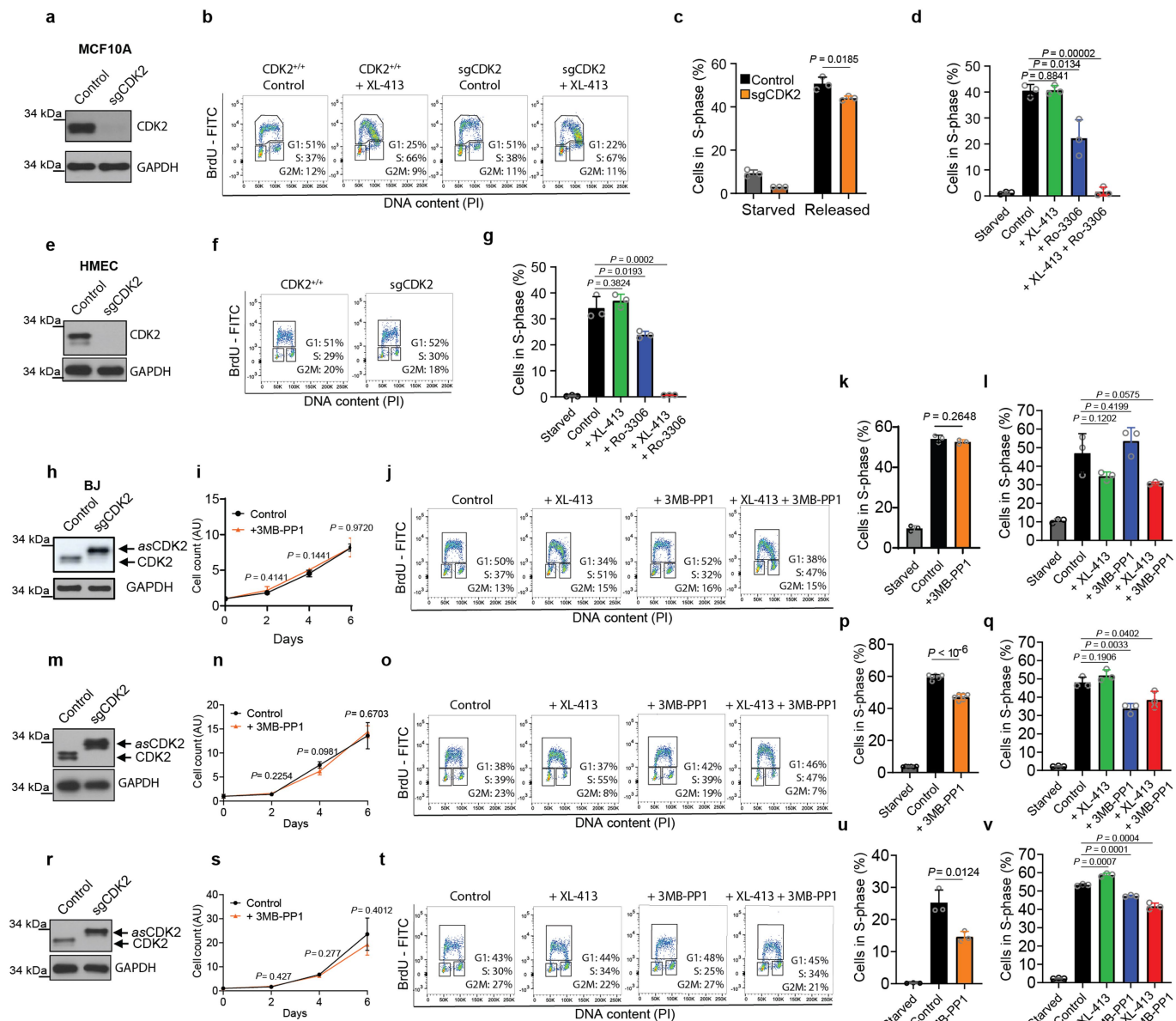
Extended Data Fig. 6 | Analyses of human CDK2-deficient cells.
a–**d**, Analyses of CDK2-knockout human mammary epithelial MCF10A cells.
a, Whole cell lysates from parental (Control) and CDK2-knockout (sgCDK2)
MCF10A cells were immunoblotted and probed with an anti-CDK2 antibody.
b, CDK2$^{+/+}$ and CDK2-knockout (sgCDK2) MCF10A cells were cultured in the
absence (Control) or presence of CDC7 inhibitor (XL-413) for 12 h. Cells were
pulsed with BrdU, stained with an anti-BrdU antibody and propidium iodide
and analyzed by flow cytometry. **c**, Parental and CDK2-knockout (sgCDK2)
MCF10A cells were arrested in G0 by growth factor deprivation (Starved) and
stimulated to re-enter the cell cycle by addition of growth factors (Released).
Cells were pulsed with BrdU after 19 h, stained with propidium iodide
and anti-BrdU antibody and analyzed by flow cytometry. **d**, CDK2-knockout
MCF10A cells were arrested in G0 and stimulated (as in **c**), in the
presence of vehicle (Control), XL-413, CDK1 inhibitor (Ro-3306), or both
inhibitors and analyzed as in **c**. **e**–**g**, CDK2-knockout human mammary
epithelial HMEC cells. **e**, Whole cell lysates from parental and CDK2-knockout
(sgCDK2) HMEC cells were immunoblotted as in **a**. **f**, Asynchronously
growing CDK2$^{+/+}$ and CDK2-knockout HMEC cells were analyzed as in **b**.
g, CDK2-knockout HMEC cells were arrested in G0 (Starved), stimulated
to re-enter cell cycle in the presence of inhibitors and analyzed as in **d**.

h–**l**, Analyses of human BJ foreskin fibroblasts expressing analog-sensitive (*as*)
CDK2 in place of the endogenous CDK2. **h**, Immunoblots of whole cell lysates of
parental and CDK2-knockout (sgCDK2) cells expressing *as*CDK2 (*as*CDK2)
probed with an anti-CDK2 antibody. *as*CDK2 migrates slower due to the
presence of 3xFlag-tag. **i**, Growth curves of *as*CDK2 cells treated with vehicle
(Control) or 3MB-PP1 (to inhibit *as*CDK2). **j**, *as*CDK2 BJ fibroblasts were
cultured with XL-413, 3MB-PP1, or both and analyzed as in **b**. **k**, **l**, *as*CDK2
cells were arrested in G0 (Starved) and stimulated with serum in the presence
of vehicle, 3MB-PP1, XL-413, or both inhibitors. Cells were analyzed as in **d**.
m–**q**, Analyses of human mammary epithelial MCF10A cells expressing
analog-sensitive CDK2 (*as*CDK2). **m**, Immunoblotting as in **h**. **n**, Growth curves
as in **i**. **o**, Analyses of asynchronously growing cells, as in **j**. **p**, **q**, analyses of
cell cycle re-entry as in **k**, **l**. **r**–**v**, Analyses of human mammary epithelial HMEC
cells expressing analog-sensitive CDK2 (*as*CDK2). **r**, Immunoblotting;
s, growth curves (as in **i**); **t**, analyses of asynchronous cells (as in **j**); **u**, **v**, analyses
of cell cycle re-entry (as in **k**, **l**). GAPDH was used as loading control.
c, **d**, **g**, **i**, **k**, **l**, **n**, **p**, **q**, **s**, **u**, **v** show mean values; *p*-values by two-sided t-test;
error bars, SD. **c**, **d**, **g**, **i**, **k**, **l**, **n**, **p**, **q**, **s**, **u**, **v**, n = 3 independent replicates; panels
a, **b**, **e**, **f**, **h**, **j**, **m**, **o**, **p**, **r**, **t**, show representative results (out of 2).
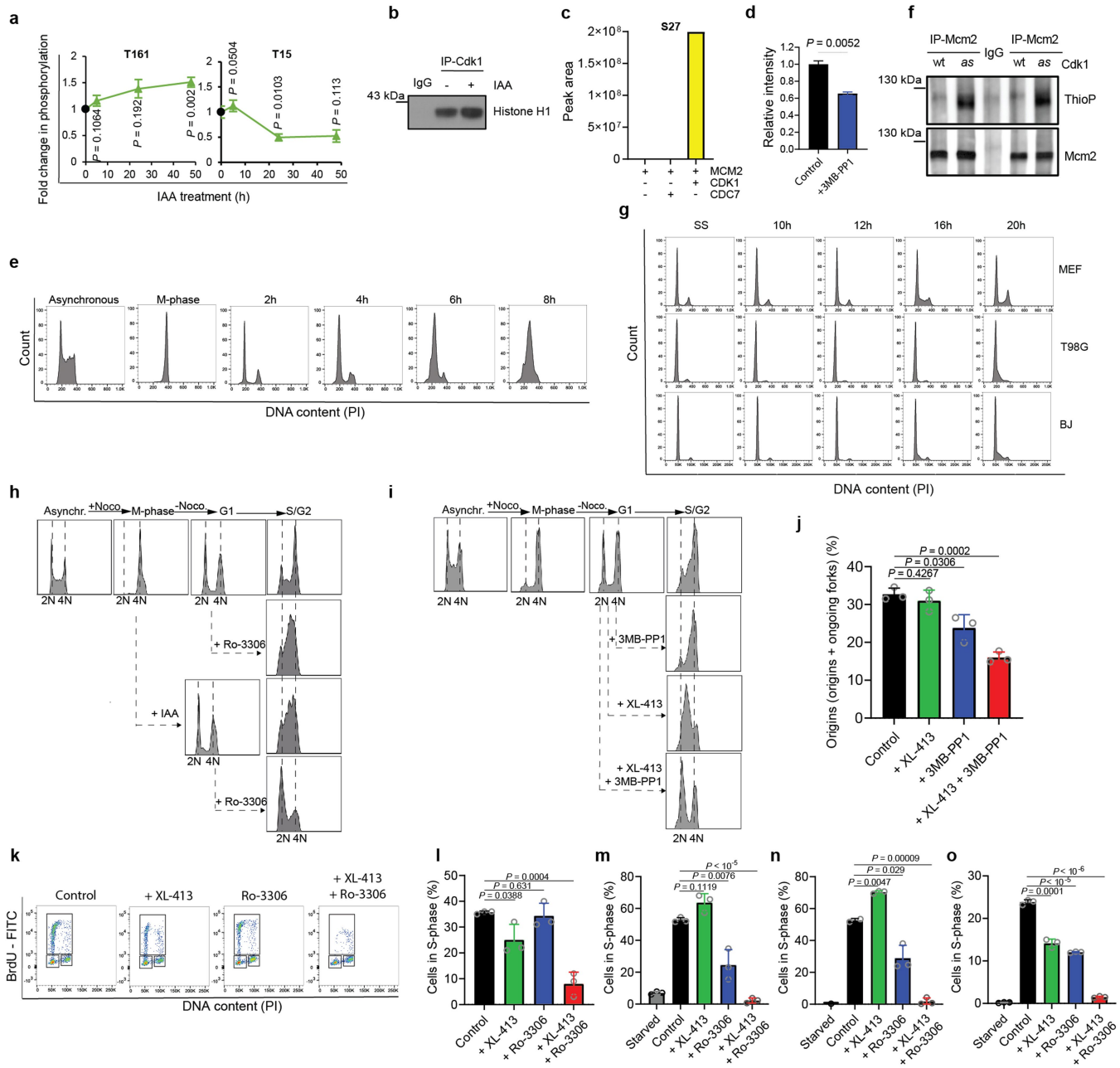
Extended Data Fig. 7 | See next page for caption.

Article

Extended Data Fig. 7 | Analyses of Cdc7-deficient cells. a, Quantification of Cdk1 phosphorylation on threonine-161 (T161) and threonine-15 (T15), using mass spectrometry. Cdc7[AID/AID]/Tir1 ESC were treated with auxin and analyzed after 5, 24 and 48 h. Black dots, phosphorylation levels at time 0. **b**, Cdk1 was immunoprecipitated (IP-Cdk1) from Cdc7[AID/AID]/Tir1 ESC treated with auxin or vehicle (−) for 24 h, and used for kinase reactions with [γ^{32}P]-ATP and histone H1 as a substrate. IgG, control immunoprecipitation. **c**, Recombinant Mcm2 was phosphorylated *in vitro* with recombinant CDK1-cyclin B1 or CDC7-DBF4 and incorporation of phosphate into serine-27 quantified by mass spectrometry. **d**, Cdk1[AS/AS] ESC were treated with 3MB-PP1 for 24 h and phosphorylation of the endogenous Mcm2 on serine-27 quantified by mass spectrometry. **e**, Wild-type ESC were arrested in mitosis by nocodazole, and released. At the indicated time-points after the release, cells were stained with propidium iodide and analyzed by flow cytometry. Asynchronous, asynchronously growing cells; M-phase, cells arrested in mitosis. **f**, In-cell phosphorylation of Mcm2 by Cdk1 during early S phase. Cdk1[AS/AS] (*as*) and wild-type (wt) ESC were synchronized in mitosis with nocodazole and released. 4 h after the release, cells were provided for 20 min with bulky ATPγS-analog, N^6-furfuryl-ATPγS, to label Cdk1 substrates. Mcm2 was immunoprecipitated (IP-Mcm2) and immunoblots probed with an anti-thiophosphate ester antibody (ThioP) to detect thio-phosphorylation of Mcm2, and with anti-Mcm2 antibody. IgG, control, immunoprecipitation from Cdk1[AS/AS] cells. Note the absence of signal for thio-phosphorylated Mcm2 in wild-type ESC cells, as expected. Shown is analysis of two independent cultures. **g**, MEFs, human glioblastoma T98G cells and BJ foreskin fibroblasts were arrested in G0 by serum starvation, and stimulated to enter the cell cycle by serum addition. At the indicated time-points after stimulation, cells were stained with propidium iodide and analyzed by flow cytometry. SS, serum starved cells. **h**, Asynchronously growing Cdk2-knockout/Cdc7[AID/AID]/Tir1 ESC (Asynchr.) were synchronized in mitosis by nocodazole (+Noco; M-phase) and released (−Noco). Upon release, Cdc7 degradation was induced by auxin (IAA) addition to account for degradation time. Two h later, when cells reached G1 phase (G1), they were treated with Cdk1 inhibitor (Ro-3306). Cells were cultured in the presence of inhibitor(s), collected after 15 h (S/G2), stained with propidium iodide and analyzed by flow cytometry along with asynchronous, M phase and G1 phase cells. Upper row, vehicle-treated cells; second, cells treated with Ro-3306; third, auxin treatment; fourth row, treatment with auxin plus Ro-3306. **i**, Asynchronously growing Cdk1[AS/AS] ESC (Asynchr.) were synchronized in mitosis by nocodazole (+Noco; M-phase) and released (−Noco). Two h later, when cells reached G1 phase (G1), they were treated with 3MB-PP1 (to inhibit Cdk1) and/or with XL-413 (Cdc7 inhibitor). Cells were cultured in the presence of inhibitor(s), collected after 12 h (S/G2) and analyzed as in **h**. Upper row, cells treated with vehicle; second, cells treated with 3MB-PP1; third, XL-413 treatment; fourth, treatment with 3MB-PP1 plus XL-413. **j**, Asynchronously growing Cdk1[AS/AS] ESC were treated with XL413 for 48 h and/or with 3MB-PP1 for the last 1 h, or with vehicle (Control), and subjected to DNA fiber analysis. Shown is the percentage of new replication origins, over the total number of forks analyzed. **k, l**, T98G cells were synchronized in M phase by nocodazole, released and treated in G1 phase with vehicle, XL-413, Ro-3306, or with both inhibitors, as in panels **h, i**. After 9 h of culture with inhibitor(s), cells were pulsed with BrdU, stained with an anti-BrdU antibody and propidium iodide and analyzed by flow cytometry (**k**). **l**, Mean percentage of S phase cells (from **k**). **m–o**, Human mammary epithelial MCF10A cells (**m**), mammary epithelial HMEC cells (**n**), and primary dermal fibroblasts (**o**) were arrested in G0 by growth factor deprivation and stimulated to re-enter the cell cycle by addition of growth factors in the presence of vehicle, XL-413, Ro-3306, or both inhibitors. Cells were pulsed with BrdU after 19 h, stained with propidium iodide and an anti-BrdU antibody and analyzed by flow cytometry along with serum-starved, G0 cells. **a, d, j, l–o** show mean values; *p*-values using two-sided t-test; Error bars, SD. **a, d, j, l–o**, n = 3 independent replicates, **b, e, g, h, i, k**, representative results (out of 2).
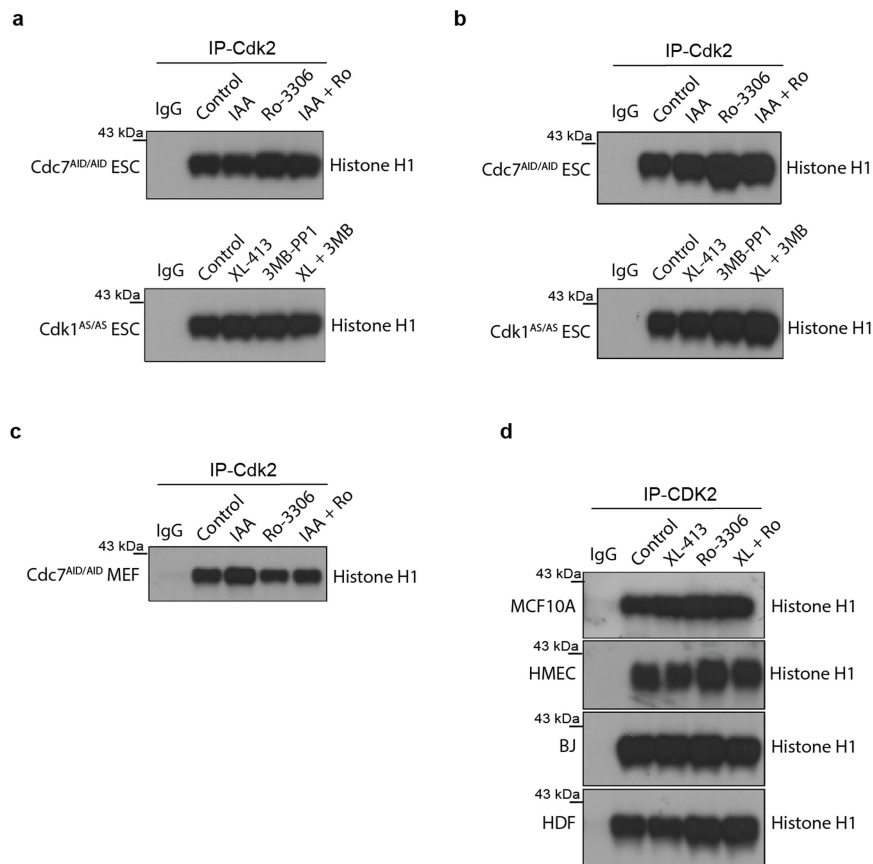
Extended Data Fig. 8 | Analyses of CDK2 activity. a, Cdc7$^{AID/AID}$/Tir1 ESC (upper panel) or Cdk1$^{AS/AS}$ ESC (lower panel) were synchronized in mitosis by nocodazole and released as in Fig. 3i and Extended Data Fig. 7h, i. Two hours after the release, Cdc7$^{AID/AID}$/Tir1 ESC were treated for 2 h with vehicle (Control), auxin (IAA), Cdk1 inhibitor Ro-3306, or with both compounds. Cdk1$^{AS/AS}$ ESC were treated for 2 h with vehicle, Cdc7 inhibitor XL-413, 3MB-PP1 (to inhibit Cdk1), or with both compounds. **b**, Upper panel: asynchronously growing Cdc7$^{AID/AID}$/Tir1 ESC were treated for 2 h with vehicle, auxin, Ro-3306 or with both compounds. Lower panel: Cdk1$^{AS/AS}$ ESC were treated for 2 h with vehicle,

XL-413, 3MB-PP1, or with both compounds. **c**, Cdc7$^{AID/AID}$/Tir1 MEFs were treated for 2 h with vehicle, auxin, Ro-3306 or with both compounds. **d**, MCF10A, HMEC, BJ fibroblasts and primary human dermal fibroblasts (HDF) were treated for 2 h with vehicle, XL-413, Ro-3306 or with both compounds. **a–d**, The endogenous Cdk2 was immunoprecipitated (IP-Cdk2) from treated cells and used for kinase reactions with [γ^{32}P]-ATP and histone H1 as a substrate. IgG, control immunoprecipitation with IgG. Note that treatment of cells with any of these inhibitors (either singly, or in combination) did not decrease the activity of the endogenous Cdk2. **a–d**, representative results (out of 2).
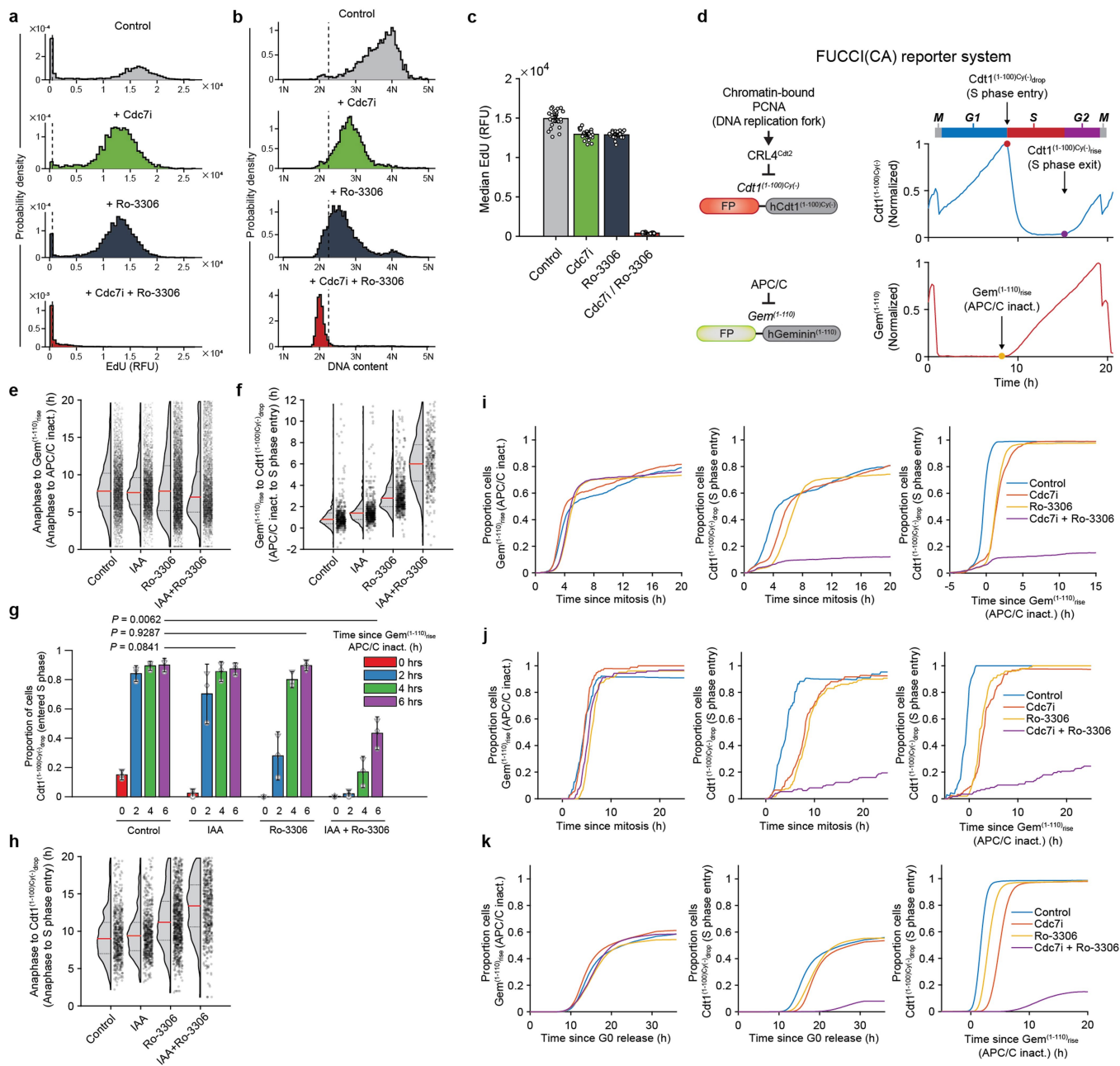
**Extended Data Fig. 9** | See next page for caption.

Extended Data Fig. 9 | Live-cell imaging. a–c, Primary human dermal fibroblasts were live-imaged and treated with vehicle (Control), CDC7 inhibitor TAK-931 (Cdc7i), CDK1 inhibitor Ro-3306, or with both inhibitors. Cells which received the inhibitor(s) starting 0–2 h after the exit of mitosis were selected for analysis. Cells were pulsed with EdU and analyzed for EdU incorporation intensity (**a**), and DNA content from Hoechst staining (**b**) 12–14 h after mitosis. Dashed vertical lines in **a** represent cutoff values for EdU-positive signal, in **b** for signal corresponding to >2N DNA significantly above 2N noise. **c**, Median EdU incorporation (from **a**). Each circle corresponds to a replicate well. **d**, FUCCI(CA) cell cycle reporter system used in the study. The system consists of fluorescent protein (FP)-tagged fragments of human Cdt1 (Cdt1$^{(1\text{-}100)\text{Cy}(\text{-})}$) and human Geminin (Gem$^{(1\text{-}110)}$). Cdt1$^{(1\text{-}100)\text{Cy}(\text{-})}$ is present during G1, and is rapidly degraded in response to origin firing at the start of S phase (Cdt1$^{(1\text{-}100)\text{Cy}(\text{-})}_{\text{drop}}$). After the S phase ends, the reporter reaccumulates (Cdt1$^{(1\text{-}100)\text{Cy}(\text{-})}_{\text{rise}}$). Gem$^{(1\text{-}110)}$ is degraded by the anaphase-promoting complex/cyclosome (APC/C) starting at anaphase and throughout G1 phase, until APC/C inactivation takes place at the end of G1 (Gem$^{(1\text{-}110)}_{\text{rise}}$). **e–h**, Asynchronously growing immortalized Cdc7$^{\text{AID/AID}}$/Tir1 MEFs expressing FUCCI(CA) reporters were live-imaged in the presence of auxin or vehicle for 4 h and then Ro-3306 was added to cells. Cells which received Ro-3306 0–2 h after the exit from mitosis were selected for analysis. **e**, Time from the end of mitosis to Gem$^{(1\text{-}110)}_{\text{rise}}$ (APC/C inactivation), in cells treated as indicated. Shown are cells with Gem$^{(1\text{-}110)}_{\text{rise}}$ by 20 h after mitosis.

f, g, Timing of Cdt1$^{(1\text{-}100)\text{Cy}(\text{-})}_{\text{drop}}$ (S-phase entry) relative to Gem$^{(1\text{-}110)}_{\text{rise}}$ (APC/C inactivation), in cells treated as above. **f**, Values for cells with Cdt1$^{(1\text{-}100)\text{Cy}(\text{-})}_{\text{drop}}$ within 12 h of Gem$^{(1\text{-}110)}_{\text{rise}}$. **g**, Fraction of cells which had Cdt1$^{(1\text{-}100)\text{Cy}(\text{-})}_{\text{drop}}$ (S phase start) at given times following Gem$^{(1\text{-}110)}_{\text{rise}}$ (APC/C inactivation). **h**, Time from the end of mitosis to Cdt1$^{(1\text{-}100)\text{Cy}(\text{-})}_{\text{drop}}$ (S-phase entry), in cells treated as indicated. In **e, f, h**, dots represent values for individual cells, pooled from independent experiments. Red horizontal lines, median values; dotted lines above and below the median, inter-quartile range. Control, vehicle-treated cells. **i, j**, Analysis of human mammary epithelial MCF10A (**i**) and osteosarcoma U2OS cells (**j**) expressing FUCCI(CA) system. Cells were live-imaged and treated with TAK-931 (CDC7i) and/or Ro-3306, or with vehicle (Control). Cells which were treated 0–2 h after the exit from mitosis were selected for analysis. Left panel: proportion of cells which underwent Gem$^{(1\text{-}110)}_{\text{rise}}$ (APC/C inactivation) over time following the end of mitosis; middle: proportion of cells which underwent Cdt1$^{(1\text{-}100)\text{Cy}(\text{-})}_{\text{drop}}$ (S-phase entry) over time following the end of mitosis; right: proportion of cells which underwent S-phase entry (Cdt1$^{(1\text{-}100)\text{Cy}(\text{-})}_{\text{drop}}$) over time following APC/C inactivation (Gem$^{(1\text{-}110)}_{\text{rise}}$). **k**, Analyses of MCF10A cells engineered as in **i**. Cells were arrested in G0, then induced to re-enter the cell cycle by re-addition of growth factors in the presence of TAK-931 and/or Ro-3306, or with vehicle, and analyzed as in **i**. **c, g**, Show mean values; error bars 2×SEM; p-values using two-sided t-test. **e–h**, n = 3 independent replicates.
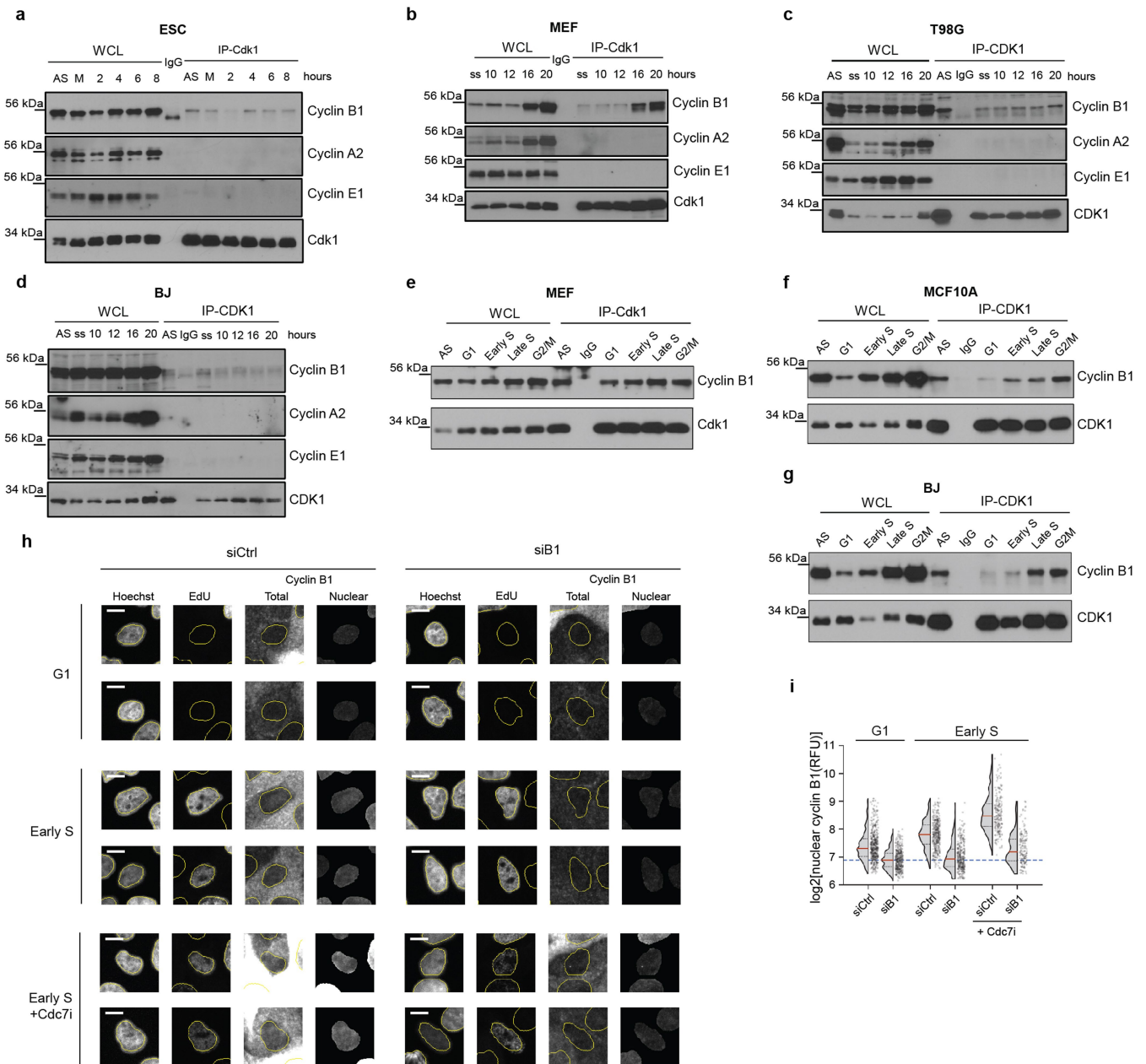
Extended Data Fig. 10 | Analyses of Cdk1-cyclin B in mouse and human cells.
a–d, ESC (**a**) were synchronized in M phase with nocodazole, released, and cell cycle progression monitored (Extended Data Fig. 7e). MEFs (**b**), human glioblastoma T98G cells (**c**), and BJ foreskin fibroblasts (**d**) were serum-starved, stimulated to re-enter the cell cycle by serum addition, and progression through the cell cycle was monitored (Extended Data Fig. 7g). Cdk1 was immunoprecipitated (IP-Cdk1) from cells at the indicated times after the release/stimulation and immunoblots probed for cyclins B1, A2 and E1, and for Cdk1. Whole cell lysates (WCL) were also immunoblotted. AS, asynchronously growing cells; M, M phase-arrested cells; ss, serum-starved cells; IgG, control immunoprecipitation. **e–g**, Asynchronously growing MEFs (**e**), human mammary epithelial MCF10A cells (**f**), and BJ fibroblasts (**g**) were stained with cell-permeant DNA-binding dyes Hoechst 33342 (MEFs) or CytoPhase Violet (MCF10A and BJ cells). Cells were sorted using FACS based on DNA content into G1, early S, late S and G2/M fractions as in Fig. 5b. Cdk1 was immunoprecipitated from flow-sorted cells and immunoblots probed with antibodies against cyclin B1 or Cdk1. Whole cell lysates (WCL) prepared from sorted cells were also immunoblotted. AS, asynchronously growing cells; IgG, control immunoprecipitation. **h**, MCF10A cells expressing Cdt1$^{(1-100)Cy(-)}$-mCherry reporter were used for combined live and fixed-cell imaging. Cells were stained with an anti-cyclin B1 antibody, and nuclear cyclin B1 staining assessed 1–2 h after mitosis in cells which had not entered S phase (G1 cells) or in cells 0.5 to 1 h after Cdt1$^{(1-100)Cy(-)}_{drop}$ (early S phase). For control of antibody specificity, cells were transfected with anti-cyclin B1 siRNA (siB1), or control siRNA (siCtrl) 24 h before fixation (cells retained sufficient cyclin B1 to progress through mitosis). Cdc7i, cells treated with the Cdc7 inhibitor, TAK-931. Total, images of cells stained for cyclin B1; nuclear, cyclin B1 nuclear signal. Cells were also stained for EdU incorporation (to confirm DNA synthesis in S but not in G1 phase nuclei) and with Hoechst (DNA stain). Scale bar, 10 µm. **i**, log$_2$ intensity of nuclear cyclin B1 staining in different treatment groups (data from Fig. 5d; G1 and early S phase cells were defined as above in **h**). Dots represent values for individual cells; red horizontal lines, median values; dotted lines above and below the median, inter-quartile range. Long dashed line denotes median nuclear cyclin B1 signal in cells treated with anti-cyclin B1 siRNA, which we consider background level. Note that anti-cyclin B1 siRNA decreased nuclear cyclin B1 staining in G1 and in early S phase cells (**h, i**), confirming the specificity of the antibody used. **a–g**, representative results (out of 2).
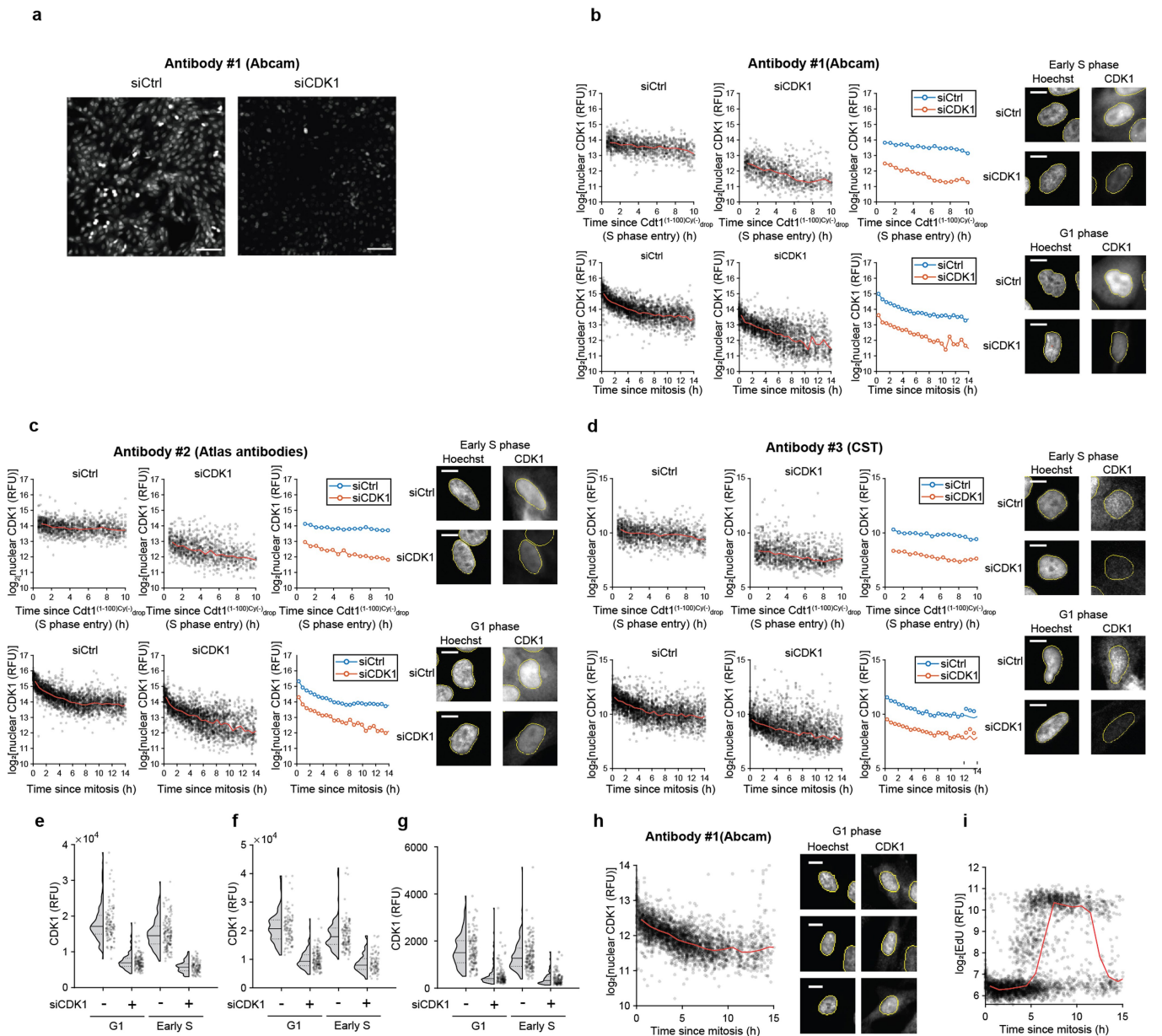
Extended Data Fig. 11 | Analyses of nuclear CDK1 during cell cycle progression. a, Immunostaining of human mammary epithelial MCF10A cells treated with control siRNA (siCtrl) or anti-CDK1 siRNA (siCDK1) for 26 h, stained with anti-CDK1 antibody #1 (Abcam). **b–d**, MCF10A cells expressing Gem$^{(1–110)}$-mVenus and Cdt1$^{(1-100)Cy(-)}$-mCherry FUCCI(CA) reporters were live-imaged and then fixed. Cells were stained with three different anti-CDK1 antibodies: (**b**) #1 from Abcam, (**c**) #2 from Atlas Antibodies, (**d**) #3 from Cell Signaling Technology (CST), and nuclear CDK1 staining was assessed. Upper rows, log$_2$ intensity of nuclear CDK1 staining at the indicated times after Cdt1$^{(1-100)Cy(-)}$$_{drop}$ (S phase start); lower panels, CDK1 nuclear intensity after the end of last mitosis. For control of antibody specificity, cells were transfected with anti-CDK1 siRNA (siCDK1), or control siRNA (siCtrl) for 6 h and then immediately imaged for 16 h. Cells depleted of CDK1 for this time retained sufficient amounts of CDK1 to progress through mitosis. Red lines represent median values within bins every 3 time-points (36 min, 12 min interval). Third panels from left show median log$_2$ intensity of nuclear CDK1 staining in control cells (blue) and cells treated with anti-CDK1 siRNA (red). Note decreased nuclear CDK1 staining (using all three antibodies) in cells transfected with anti-CDK1 siRNA, which confirms the specificity of the antibodies. Right panels (images of cells) depict examples of nuclear CDK1 staining used for quantification in the previous panels. Upper panels (set of 4 pictures labelled

'early S phase'), Hoechst (DNA) and CDK1 staining for cells fixed 48 min (4 time-points) after Cdt1$^{(1-100)Cy(-)}$$_{drop}$ (S phase start); lower panels labelled 'G1 phase', cells fixed 3 h after the end of last mitosis in G1. Cells were transfected with control siRNA or anti-CDK1 siRNA. CDK1 depletion (siCDK1) decreased nuclear CDK1 staining in G1 and early S phase cells. **e–g**, Another representation of values from **b–d**, for cells in G1 (3-4 h after mitosis) and early S phase (0-1 h after Cdt1$^{(1-100)Cy(-)}$$_{drop}$), transfected with control siRNA (siCDK1 -) or with anti-CDK1 siRNA (siCDK1 +) and stained with anti-CDK1 antibody #1 (**e**), #2 (**f**) or #3 (**g**). Dots show values for individual cells, horizonal lines depict median values, dotted lines above and below the median represent inter-quartile range. **h–i**, Live and fixed-cell analysis of primary human dermal fibroblasts, similar to **b–d**. **h**, Since cells did not express the FUCCI reporters, we analyzed nuclear CDK1 staining relative to the end of last mitosis (left panel). Right panels (cell images) show nuclear CDK1 staining in cells stained 3 h after the end of last mitosis (labelled G1 phase). Nuclei were stained with Hoechst. **i**, log$_2$ of EdU incorporation in cells from the left panel (to illustrate their cell cycle progression), pulsed with EdU for 8 min prior to fixation; EdU-high cells correspond to S phase cells, EdU-low to G1 or G2 cells. **h–i**, Red lines represent median values within bins every 6 time-points (60 min, 10 min interval). Scale bars, 100 μm (**a**); 10 μm (**b–d, h**).
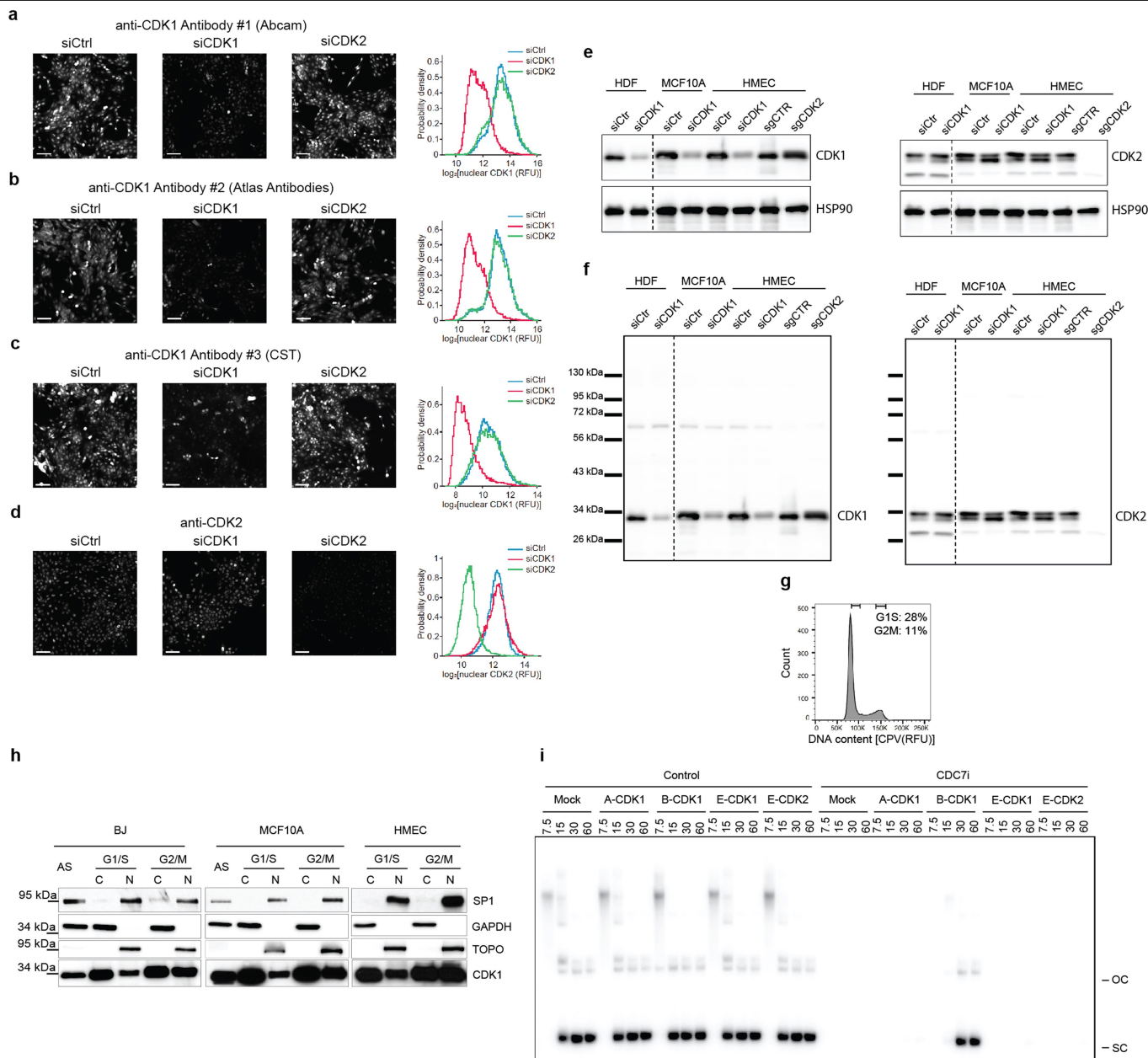
Extended Data Fig. 12 | Analyses of anti-CDK1 antibody specificity and subcellular fractionation. a–d, Immunostaining of MCF10A cells transfected with control siRNA (siCtrl), anti-CDK1 siRNA (siCDK1), or anti-CDK2 siRNA (siCDK2) for 24 h, stained with (**a**) anti-CDK1 antibody #1 (Abcam), (**b**) anti-CDK1 antibody #2 (Atlas Antibodies), (**c**) anti-CDK1 antibody #3 (Cell Signaling Technology, CST) or (**d**) anti-CDK2 antibody. Scale bars, 100 μm. Quantification of fluorescence intensity within the nuclei is shown on the right of each panel. Note that the anti-CDK1 immunofluorescence signal decreases upon depletion of CDK1 (siCDK1), but not following depletion of CDK2 (siCDK2). The anti-CDK2 signal decreases after depletion of CDK2 (siCDK2) but not of CDK1 (siCDK1). **e, f,** primary human dermal fibroblasts (HDF), MCF10A and HMEC cells and were transfected with control siRNA (siCtrl) or anti-CDK1 siRNA (siCDK1) for 48 h. Protein lysates were immunoblotted with anti-CDK1 antibody #1 (Abcam, left panel) or anti-CDK2 antibody (right panel). Lysates from CDK2-knockout (sgCDK2) and control (sgCTR) HMEC cells were immunoblotted in parallel. HSP90 was used as a loading control. The CDK1 signal decreased following depletion of CDK1, while the CDK2 signal remained unaffected. Knockout of CDK2 abrogated the CDK2 signal, but not the CDK1 signal. Panel **e** shows bands corresponding to CDK1, CDK2 and HSP90, panel **f** full-length blots probed with anti-CDK1 and anti-CDK2 antibodies. Dashed vertical lines indicate that the middle portions of the blots were spliced out;

first two left lanes (HDF cells) were exposed for a longer time than the rest of the blot. **g, h,** Asynchronously growing human BJ foreskin fibroblasts and human mammary epithelial MCF10A and HMEC cells were stained with cell-permeant DNA-binding dye CytoPhase Violet. Cells were sorted using FACS, based on DNA content, into G1/S and G/M fractions. Cytoplasmic and nuclear fractions were prepared from cells, resolved on gels (10 μg of cytoplasmic, 20 μg of nuclear) and immunoblots probed for CDK1 (antibody #1, Abcam), GAPDH (a cytoplasmic marker), SP1 and topoisomerase I (TOPO) (both markers of the nuclear fraction; in BJ cells TOPO band migrated at ~75 kD). **g,** example of gating strategy for flow-sorting (BJ cells), **h,** immunoblot analysis; C, cytoplasmic fraction; N, nuclear fraction; AS, whole cell lysates from asynchronously growing non-sorted cells. In agreement with immunostaining (Extended Data Fig. 11), we detected nuclear CDK1 in G1/S cells. **i,** DNA replication assays in nucleus-free *Xenopus* egg extracts (see Fig. 5e for quantification). Extracts were treated with Cdc7 inhibitor PHA-767491 (CDC7i) or with DMSO (Control). The indicated recombinant cyclin-CDK complexes were added, and nascent strand DNA synthesis assessed by incorporation of [α-32P]-dATP at 7.5, 15, 30 and 60 min following replication initiation. OC, open circular plasmid; SC, supercoiled plasmid. **a–h** Show representative results (out of 2), **i** out of 3.

Corresponding author(s): Piotr Sicinski

Last updated by author(s): March 13, 2022

Reporting Summary

Nature Research wishes to improve the reproducibility of the work that we publish. This form provides structure for consistency and transparency in reporting. For further information on Nature Research policies, see our Editorial Policies and the Editorial Policy Checklist.

Statistics

For all statistical analyses, confirm that the following items are present in the figure legend, table legend, main text, or Methods section.

n/a	Confirmed	
☐	☒	The exact sample size (n) for each experimental group/condition, given as a discrete number and unit of measurement
☐	☒	A statement on whether measurements were taken from distinct samples or whether the same sample was measured repeatedly
☐	☒	The statistical test(s) used AND whether they are one- or two-sided *Only common tests should be described solely by name; describe more complex techniques in the Methods section.*
☒	☐	A description of all covariates tested
☒	☐	A description of any assumptions or corrections, such as tests of normality and adjustment for multiple comparisons
☐	☒	A full description of the statistical parameters including central tendency (e.g. means) or other basic estimates (e.g. regression coefficient) AND variation (e.g. standard deviation) or associated estimates of uncertainty (e.g. confidence intervals)
☐	☒	For null hypothesis testing, the test statistic (e.g. F, t, r) with confidence intervals, effect sizes, degrees of freedom and P value noted *Give P values as exact values whenever suitable.*
☒	☐	For Bayesian analysis, information on the choice of priors and Markov chain Monte Carlo settings
☒	☐	For hierarchical and complex designs, identification of the appropriate level for tests and full reporting of outcomes
☒	☐	Estimates of effect sizes (e.g. Cohen's d, Pearson's r), indicating how they were calculated

Our web collection on statistics for biologists contains articles on many of the points above.

Software and code

Policy information about availability of computer code

Data collection	NIS elements BD FACSDiva
Data analysis	DNA fiber and immunoblot analyses were performed using the Fiji Software v1.0 Mass spectra were processed using a SEQUEST-based pipeline as described in Huttlin, E. L. et al. Cell 143, 1174-1189 (2010). Automated image analysis was performed using custom MATLAB scripts as described in Cappell, S. D. et al. Cell 166, 167-180 (2016). Flow cytometry analyses were performed with FlowJo v10.7.1

For manuscripts utilizing custom algorithms or software that are central to the research but not yet described in published literature, software must be made available to editors and reviewers. We strongly encourage code deposition in a community repository (e.g. GitHub). See the Nature Research guidelines for submitting code & software for further information.

Data

Policy information about availability of data

All manuscripts must include a data availability statement. This statement should provide the following information, where applicable:

- Accession codes, unique identifiers, or web links for publicly available datasets
- A list of figures that have associated raw data
- A description of any restrictions on data availability

Source data for mass spectrometry analyses has been deposited to the ProteomeXchange Consortium via the PRIDE partner repository with the dataset identifier PXD025625.
ProteomeXchange title: The role of Cdk1-cyclin B in G1/S transition revealed by chemical genetic inhibition of Cdc7. ProteomeXchange accession: PXD025625.
Project Webpage: http://www.ebi.ac.uk/pride/archive/projects/PXD025625. Raw imagining datasets are available upon request.

Field-specific reporting

Please select the one below that is the best fit for your research. If you are not sure, read the appropriate sections before making your selection.

☒ Life sciences ☐ Behavioural & social sciences ☐ Ecological, evolutionary & environmental sciences

For a reference copy of the document with all sections, see nature.com/documents/nr-reporting-summary-flat.pdf

Life sciences study design

All studies must disclose on these points even when the disclosure is negative.

Sample size	We determined sample size based on sufficient statistics. The sample size should be more than 3 across the manuscript.
Data exclusions	No data was excluded from the experiments.
Replication	Yes, the experimental findings were reliably reproduced. All experiments in which p-values are present have been carried out with at least 3 replicates. All experiments were independently reproduced at least twice.
Randomization	Not relevant to this study. All in vivo experiments were carried out using mice which received exactly the same treatment. The mice used in these experiments all had the same genotype and genetic background.
Blinding	Blinding was not relevant to the study. Readout is not subject to experimenter bias. All mice were receiving the same treatment and had the same genotype.

Reporting for specific materials, systems and methods

We require information from authors about some types of materials, experimental systems and methods used in many studies. Here, indicate whether each material, system or method listed is relevant to your study. If you are not sure if a list item applies to your research, read the appropriate section before selecting a response.

Materials & experimental systems

n/a	Involved in the study
☐	☒ Antibodies
☐	☒ Eukaryotic cell lines
☒	☐ Palaeontology and archaeology
☐	☒ Animals and other organisms
☒	☐ Human research participants
☒	☐ Clinical data
☒	☐ Dual use research of concern

Methods

n/a	Involved in the study
☒	☐ ChIP-seq
☐	☒ Flow cytometry
☒	☐ MRI-based neuroimaging

Antibodies

Antibodies used	Flag mAb (clone: M2, Sigma: F3165) Flag (clone: M2, Sigma: F1804) Gapdh (CST: D16H11) Mcm2 (Abcam: ab4461) Mcm2 phospho-S27 (Abcam: ab109459) Mcm2 phospho-S40 (Abcam: ab133243) Mcm2 phospho-S53 (Epitomics: 3386-1 Mcm2 antibody (Proteintech: 10513-1-AP) CDC7 (MBL: K0070-3S) Cdc7 (Abcam: ab229187) Cyclin A (SCBT: sc-596) Cyclin B1 (Abcam: ab181593), cyclin B1 (CST: 12231) Cyclin E1 (SCBT: sc-481), Cdk1 (Abcam: ab71939), CDK1 (Abcam, ab133327) Cdk2 (SCBT: sc-163) CDK2 mAb (CST: 18048) CDK2 (Abcam ab32147) beta-actin (Sigma: A5441) HSP90 (CST 4877). Thiophosphate ester (Abcam: ab92570)

Chk1 (CST: 2360S)
Chk1 phospho-S317 (CST: 12302S)
Chk1 phospho-S345 (CST: 2348S)
KAP1 (Bethyl: A300-274A-M)
KAP1 phospho-S824 (Bethyl: A300-767A-M)
p53 (SCBT: sc-393031)
Rb (CST: 9313S)
goat anti-rabbit Alexa Fluor 488 (Thermo Fisher Scientific: A-11034)
goat anti-rabbit Alexa Fluor 647 (Thermo Fisher Scientific: A-21245)
goat anti-mouse Alexa Fluor 488 (Thermo Fisher Scientific: A32723)
goat anti-mouse Alexa Fluor 647 (Thermo Fisher Scientific: A32728)

Validation	The described antibodies were validated by manufacturers or validated during our previous studies. Statements of antibody validation are present on the manufacturer websites along with relevant references. In addition, CDK1 antibody was further validated during this study against CDK1-CDK2 cross-reactivity.

Eukaryotic cell lines

Policy information about cell lines

Cell line source(s)	MCF10A (ATCC: CRL-10317) T98G (ATCC: CRL-1690) U2OS (ATCC: HTB-96) HDF (Sigma: 106-05A) EMT6 (ATCC: CRL-2755) 4T1 (ATCC: CRL-2539) BJ fibroblasts (gift from Dr. William Hahn's Laboratory at Dana-Farber Cancer Institute) HMEC (gift from Dr. Thomas Roberts' Laboratory at Dana-Farber Cancer Institute) 4T07 (gift from Dr. Kornelya Polyak's Laboratory at Dana-Farber Cancer Institute)
Authentication	The MCF10A, T98G, U2OS and EMT6 cell lines were purchased directly from ATCC and thus not further authenticated. The Human Dermal Fibroblast (HDF) cells were purchased directly from Sigma and thus not further authenticated.
Mycoplasma contamination	Cells used in all experiments were routinely tested for mycoplasma contamination and only mycoplasma-negative cells were used for experiments.
Commonly misidentified lines (See ICLAC register)	No commonly misidentified cell lines were used in the study.

Animals and other organisms

Policy information about studies involving animals; ARRIVE guidelines recommended for reporting animal research

Laboratory animals	Mice generated in this project were created using V6.5 ES cells which are derived from Mus musculus of mixed genetic background (C57BL/6 with Sv129; 1:1). Male and female, 4-8 week old animals were used.
Wild animals	The study did not involve wild animals.
Field-collected samples	The study did not involve samples collected in the field.
Ethics oversight	Dana-Farber Cancer Institute Institutional Animal Care and Use Committee (IACUC) Harvard Medical School Institutional Animal Care and Use Committee (IACUC)

Note that full information on the approval of the study protocol must also be provided in the manuscript.

Flow Cytometry

Plots

Confirm that:

☒ The axis labels state the marker and fluorochrome used (e.g. CD4-FITC).

☒ The axis scales are clearly visible. Include numbers along axes only for bottom left plot of group (a 'group' is an analysis of identical markers).

☒ All plots are contour plots with outliers or pseudocolor plots.

☒ A numerical value for number of cells or percentage (with statistics) is provided.

Methodology

Sample preparation	Cells were pulsed BrdU for 30 minutes (ES cells) or 1 hour (MEFs, BJ fibroblasts, keratinocytes, cardiomyocytes), then stained with an anti-BrdU antibody and with propidium iodide followed by flow cytometry. Pulse-chase experiments were carried out as previously described in Liu, L. et al. Nat Cell Biol 19, 177-188 (2017).

Instrument	BD LSRFortessa
Software	BD FACSDiva
Cell population abundance	In most cases data was obtained from at least 10000 cells.
Gating strategy	Single cells described on the PI-H to PI-A signal; 2N and 4N (BrdU-negative) populations gated on the basis on propidium iodide signal in BrdU-negative cells; BrdU-positive (S-phase) gate determined based on BrdU-positive vs. noBrdU (BrdU-negative) cell populations.

☒ Tick this box to confirm that a figure exemplifying the gating strategy is provided in the Supplementary Information.